Photoreaction Dynamics of Molecular Adsorbates on Semiconductor and Oxide Surfaces

Richard Osgood

Department of Applied Physics and Applied Mathematics, Columbia University, New York, New York 10027

Received January 13, 2006

Contents

1. Introduction

In this article, we will discuss the dynamics of UV photoreactions on single-crystal, semiconductor, and insulator surfaces. We will focus this discussion of surface dynamics by considering mainly the system of weakly to moderately bonded species on the reconstructed surfaces of oxides and semiconductors. We examine these two classes of substrate crystals here because both have band gaps at zone center and both exhibit a combination of ionic and covalent bonding. Furthermore, since extensive and comprehensive studies have been done on semiconductor surfaces, those results allow us to project what we can anticipate in oxide systems as an increasing number of photodynamics measurements are made on these systems. Note that as in gas-phase photochemistry measurements, these studies generally have used some form of temporally modulated lasers, typically short-pulse sources, since they are ideal for time-of-flight-based studies.

Professor Richard Osgood began his research into laser excitation and probing of chemical physics phenomena during his Ph.D. studies in the MIT Department of Physics under Professor Ali Javan from 1969 to 1973. He continued this work while at MIT Lincoln Laboratory from 1973 to 1981. He then moved to Columbia University, where he is Higgins Professor in the Department of Applied Physics and Mathematics and the Department of Electrical Engineering. While at Lincoln Laboratory, he began research into the basic chemical physics underpinning of laser-initiated surface reactions. At present, his work with students and postdocs in chemical physics is focused on understanding light–surface interactions and considers such topics as photoexcited chemical dynamics on metal, metal oxide, and semiconductor surfaces, the surface molecular physics of atomic-layer processes, proximal probing of nanoparticle reactions, and ultrafast studies of quantized, surface-electron phenomena.

The underlying phenomenon addressed by this review is the photochemistry of molecular adsorbates on surfaces. Surface photochemistry is the basis of a wide variety of extremely important technological processes and applications.[1] For example, light-induced surface reactions on TiO_2 are the basis for several important environmental remediation methods and for several proposed methods of solar energy generation.[2,3] As a result of this intense interest, there are many excellent reviews of surface photochemistry, including

10.1021/cr050175x CCC: $59.00
Published on Web 09/26/2006

those that have practical as well as a fundamental science orientation.[4−7] It is clearly impossible to review this large body of literature, and thus, we focus here instead on the specific area of the molecular dynamics of photoreactions. Photoreaction dynamics studies have a much more recent history, since they largely rely on optical excitation and probing methods, which have their origin in laser photochemistry and rely on the synthesis of these techniques with ultrahigh-vacuum methods and probes. In addition, our review will be restricted to examining reactions of nonmetallic surface substrates. However, since the studies we will describe are intimately related to concomitant studies on metal, particularly single-crystal metal surfaces, it is important to mention at the outset some of these studies and the articles in this area; clearly however, it is not possible to cite all of this fine work, even in the somewhat restrictive area of photodynamics.

Single-crystal metal surfaces were used extensively in early photodynamics experiments because of their applicability to heterogeneous catalysis. For example, mechanistically, these studies uncovered the importance of photoexcited electrons in initiating reactions[8] and the role of the surface work function[4,9] in setting the threshold for this photoreaction process. Similarly, metal surfaces were shown to quench excited molecular states[8] and, hence, photoreactions. There are several excellent reviews of these phenomena, on metal and other surfaces, and these[4,5,10] are given in the references to this chapter. Metal surfaces have also been used to show a host of other important photoreaction processes, including surface-aligned photochemistry,[11] hot-fragment-initiated secondary reactions,[12,13] surface stabilization,[4,8,14] etc. Metal surfaces have also been an important "testing ground" to explore the physics of optically induced desorption of strongly bound,[15,16,17] that is, strongly chemisorbed, molecules or atoms; these systems have many of the characteristics of dissociation seen in desorption induced by electronic transitions (DIET),[18] a process not covered directly by this review. Finally, while this chapter and many of the papers just cited consider linear photochemistry, there is a large body of work that relies on the use of ultrafast lasers to initiate *nonlinear* surface photochemistry on metal surfaces. One of these, DIMET(dissociation induced by multiple electron transfer),[19,20] is in many ways a multiple-electron analogue to the single-photoelectron-initiated chemistry to be discussed below.

Alkyl halides have been chosen as model adsorbate species for many of these studies because their excitation chemistry allows comparison of the two main dissociation processes that typically occur for these systems; namely, direct photodissociation of adsorbed species by incident ultraviolet radiation and dissociative electron attachment (DEA), which involves bond scission via attachment of low-energy photoelectrons generated in the substrate crystal. Competition between these processes is seen most clearly on semiconducting surfaces[21] such as GaAs (110), since its band gap is in an energy range thaat enables excitation of surface photoelectrons at near-UV wavelengths.[10,22] In addition, the surface reconstructions on GaAs surfaces are well-studied and are known to lead to orientation of molecular adsorbates.[23] Oxide surfaces also have well-defined surface reconstructions.[24,25] Their electronic structure, however, has in many important cases, such MgO or Al_2O_3, much larger band gaps. As will be discussed below, such large gaps inhibit excited-state quenching and photogeneration of carriers, and as a result, direct photodissociation is dominant on these particular oxide surfaces. The dynamics of photomediated processes in these adsorbate/substrate systems are a result of several interrelated phenomena, including excitation by either photons or surface electrons and the dependence of this excitation on the initial molecular and crystal degrees of freedom, loss of excitation to the surface via resonant-electron-transfer processes, and perturbation of the isolated-molecule half-collision on the excited-state potential surface. The use of laser sources has been a key element in investigating photodynamics, since the degree of excitation can be sufficiently high that large concentrations of fragments and other transient species can be prepared, thus allowing easy probing of reaction transients or products.

One particularly important direction of research has been to examine the interrelation of adsorbed-molecule orientation with its photoexcitation dynamics. These studies have been extensively pursued on metals,[26] insulators,[27] and semiconductors[22] to delineate reaction mechanisms for each of these surfaces. This experimental work on molecular-orientation-resolved photochemistry has made effective use of angle-resolved, time-of-flight mass spectrometry and has enabled the observation of striking phenomena, such as site-specific chemistry and site-specific fragmentation, as well as their coverage and photon-energy dependence. Many of these studies have involved diatomics or quasidiatomics because of their clear photofragmentation patterns.

Our plan for this chapter is as follows: We will first outline the experimental methods of photodynamics and the physical properties of many of the model crystal substrates to be discussed here. We will then review the current understanding and recent research on the chemical physics of reaction dynamics on one semiconducting surface, GaAs (110), and thus use this surface as a prototypical system to discuss the central physics of surface photodynamics. In this section will be comments on fragment kinetic energy, internal (vibrational and electronic) energies, and fragment angular distributions and their implications insofar as reaction mechanisms and photofragmentation are concerned. We will focus our presentation heavily, but not exclusively, on alkyl halides as model molecules on this wide-band gap semiconductor surface. Finally we will then describe photodynamics on three model metal oxide crystal surfaces, including wide-, medium-, and narrow-band gap substrates. We will then conclude with a summary and a prospectus for future work.

2. Experimental Methods

Careful surface dynamics studies are at their core ultrahigh-vacuum surface science. They require a clean, fully ordered surface that is well-characterized in terms of structure and composition. They also require the electron, X-ray, and thermal desorption tools necessary to fully characterize and prepare these near-ideal surfaces. Thus far, studies of surface photodynamics have used almost exclusively temporally modulated lasers to examine the fragments ejected from the surface during irradiation. The most widely used dynamics measurement technique, time-of-flight mass spectrometry, employs nanosecond pulsed lasers because of the large number of photons per pulse and because the short-time-duration desorption pulse allows one to distinguish photofragments ejected from the surface at typical energies of 0.1−5 eV. Since $\sim 10^{-13}$ s is required for a typical low-mass-weight fragment to exit the surface, the photodesorption process is effectively instantaneous, even during short optical

pulses. By employing a tunable laser for excitation, it is possible to investigate the threshold energies for fragment formation. Finally, a crucial measurement tool is the use of angle- and time-resolved mass-spectroscopic measurements of the fragment velocity.[11,28] Angular-resolved TOF measurements allow one to probe the influence of the surface structure on the surface dynamics and to characterize the desorption event by the fragment energy.

More recently, scanning tunneling microscopy (STM) methods[29] have been applied to the photodynamics measurements. In contrast to the mass-spectroscopic methods, STMs have been used to study the detailed spatial distribution of fragments retained on the surface. In this case, one examines the atomic location of fragments retained after irradiation of, typically, an isolated adsorbed species. Through examination of the fragment, say, Br from photodissociated CH_3Br, one can infer information on the site of the parent molecule and the trajectories of its photofragments. Because of the constrained open space within the STM region, the irradiation optical train can be a major factor in experimental design.

3. Materials Systems

3.1. Surface Atomic and Electronic Structure on Ionic or Covalent Surfaces

As will be discussed in subsequent sections, the surface structure of the "substrate", which supports the target adsorbate molecule, plays a crucial role in many dynamical processes, as does the electronic structure of this same substrate crystal. Excellent overviews of the surface structure for semiconductors and insulators are provided in several introductory texts on surface science[24,30,31] and in several complete survey papers;[25,32] we will thus not attempt to give a detailed treatment here. Instead, we will attempt merely to illustrate the relevant physics of these surfaces by presenting several examples that are relevant in the discussion of the dynamics below.

3.1.1. GaAs (110)

GaAs (110) is chemically stable over a broad temperature range and provides a nonpolar, stoichiometric surface. After exposure to a reactive environment, it can be restored to a satisfactory state in situ via sputter-annealing. The structure of GaAs (110) as depicted by Duke, et al,[33] is shown in Figure 1. The figure also shows the orientation of the surface with respect to the usual Miller indices as well as the two-digit diffraction surface vectors. Note that, in general, the surface relaxation of the (110) surface of compound semiconductors is largely independent of the semiconductor ionicity;[32] thus, the (110) surfaces of other compound semiconductors, whether III−V or II−VI, have similar atomic structure but somewhat different electronic properties.

Electronically, both the Ga- and As-derived surface bands of GaAs (110) are located near the conduction-band minimum and the valence-band maximum, respectively.[30] The locations of donating substrate surface bands on GaAs (110), in the vicinity of the band gap, are determined by surface relaxation. Specifically, the (110) surface of GaAs is structurally asymmetric due to the inward rotation of the topmost As−Ga chain, as illustrated in Figure 1. During the surface relaxation, GaAs (110) rehybridizes so as to leave one Ga p orbital near the conduction band minimum (CBM) unoccupied and oriented approximately perpendicular to the plane defined by the three GaAs bonds. The analogous hybrid orbital on the As atom is occupied, with its energy just below the valence band maximum. Optical excitation of the semiconductor interfacial region dominantly excites electrons in the bulk conduction band; these electrons then relax into a combination of the normally unoccupied bulk and surface states at the CBM. The dynamics of electrons in the Ga-orbital-derived surface state following optical excitation of bulk bands has been observed directly using two-step photoemission on GaAs (110).[34]

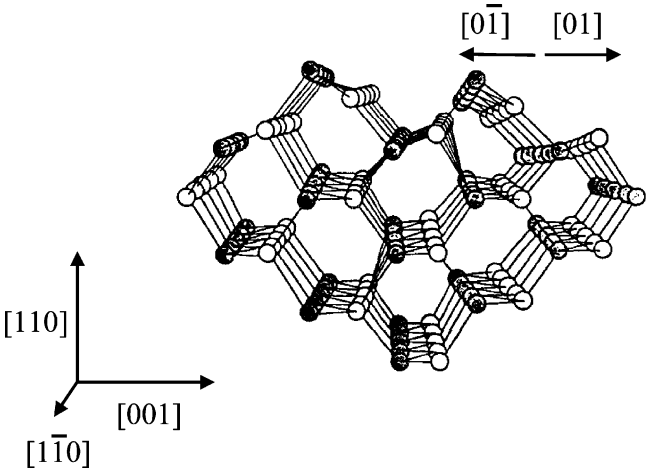

Figure 1. A schematic side view of the relaxed (110) face of a compound semiconductor with zincblende structure. In this case, the top layer rotates so as to thrust the As atom (●) outward and the Ga atom (○) inward. The relaxation in the second layer is exaggerated for visualization. The orientation of surface with respect to the crystal Miller indices is shown, as well as the two-digit surface directions from dynamic LEED measurements. Reprinted from ref 33, copyright 1988, with permission from AVS: The Science and Technology Society.

3.1.2. Fe_2O_3

Single-crystal hematite has become the de facto model mineralogical substrate for reactivity studies with environmentally relevant molecular species.[35−37] Single-crystal hematite, α-Fe_2O_3 (0001), has several different well-studied surface reconstructions[38,39] that are obtained by varying the thermal annealing temperatures and oxygen partial pressures during the heating cycle. These surfaces are magnetite, Fe_3O_4 (111)−(2 × 2); hematite, Fe_2O_3 (0001); and the so-called "biphase", Fe_2O_3 (0001) + Fe_xO. It is interesting that previous research, including that using a synchrotron, an STM, and laboratory-based UHV probes, has shown that these three common terminations exhibit distinctly different reactivity toward different molecular adsorbates. The most chemically active was found to be the Fe_3O_4 (111)−(2 × 2) selvedge formed on the (0001) plane of the α-Fe_2O_3 crystal. A schematic representation, originally presented by Joseph, et al.,[40] showing the current understanding of the termination of the Fe_3O_4 (111)−(2 × 2) surface, is presented in Figure 2. This surface is terminated by a 1/4 monolayer of tetrahedrally coordinated Fe^{3+} cations, which may act as strong Lewis acid sites. This termination results in a 1/4 monolayer of the hexagonal close-packed surface oxygen atoms remaining uncapped by the surface iron atoms; these are identified as O_a in Figure 2. This surface has a small, that is, ∼0.2 eV, band gap and is, thus, conducting at room temperature.

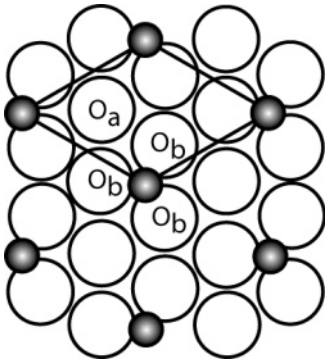

Figure 2. Top view of the Fe_3O_4 (111)−(2 × 2) surface (a = 5.92 Å), which can be formed on an Fe_2O_3 (0001) surface. The solid-black spheres are Fe atoms. The oxygen atoms marked by O_b are capped by 1/4 of a monolayer of Fe^{3+} cations, whereas those marked by O_a are uncapped. In the bulk, these unsaturated atoms have a bond perpendicular to the surface. The oxygen sites identified by O_a are likely to be abstracted in surface reactions. Image and terminology reprinted from ref 40, copyright 1999, with permission from Elsevier.

3.1.3. TiO_2 (110)

The rutile TiO_2 surface is thought to be the most thermodynamically stable surface of crystalline TiO_2; in many ways, it has become the prototypical metal oxide surface for heterogeneous chemistry studies.[25] A depiction of this surface, taken from a recent article by Henderson,[41] is shown in Figure 3. As is shown, the surface consists essentially of a bulk-terminated slab of atoms. In bulk rutile, Ti is bonded in 6-fold octahedra cation sites, whereas O is in 3-fold coordinated anionic sites. At its surface, the crystal consists of 2-fold coordinated O^{2-} sites and 5-fold Ti^{4+} sites; the former acts as a Lewis base, and the latter, as a Lewis acid. This structure has 5.2×10^{14} sites/cm^2 for each species.[42] The surface is capped with rows of doubly bonded oxygen atoms along the [110] direction. The electronic structure of the (100) surface is autocompensating, and thus, excess charge is transferred from the cation dangling bonds to the anion bonds. This charge rearrangement results in the cation states' being empty and the anion states' being full. The surface may be prepared *in vacuo* to assume its (1 × 1) relaxation by sputter-annealing cycles in the presence of oxygen. In this relaxed state, the oxygen atoms are relaxed inward to have a lattice constant of 1.71 A instead of 1.95 A, the relaxation of surface Ti is more complex, and different sets of Ti atoms have both inward and outward relaxation.

The band gap of the rutile form of TiO_2 is 3.08 eV. When the crystal is annealed *in vacuo*, it develops oxygen vacancies to become n-type and conducting, which allows it to be used with UHV electron probes.[43] Under strong reducing conditions, the (1 × 1) surface can assume a (1 × 2) reconstruction. Finally, note that the rutile and anatase crystal types have significantly different chemical properties; in particular, rutile is considered to be less photoactive. Despite this fact, unlike many of the other surfaces discussed in this section, the photoexcited charge-transfer chemistry on rutile TiO_2 has been studied extensively and in much detail; this chemistry has been found to be surprisingly subtle.[44] For example, many photoreactions involve electron scavenging by adsorbed O_2 as a means of reoxidizing surface oxygen vacancy sites.

3.2. Adsorbate Surface Phases

A major question in surface dynamics is related to the structural phase of the adsorbate molecules, in which phase includes both the order within the adsorbed-molecular layer and the orientation with respect to the substrate. Clearly, as in the case of the crystal surface structure, adsorbate phase is in itself a major research area. As a result, we provide a brief overview of what is known in the case of one physisorbed-polar-molecule model system and use it to illustrate the central issues, which will be encountered elsewhere in this article.

The unusually complete studies of adsorption of CH_3Br on GaAs (110)[45] have made it a useful model adsorbate system. Because the methyl bromide has been found to only physisorb to a GaAs surface, dosing must be accomplished at ∼85 K; the adsorbed layer is then, except for limited reactions at any defect sites, found to consist of the intact

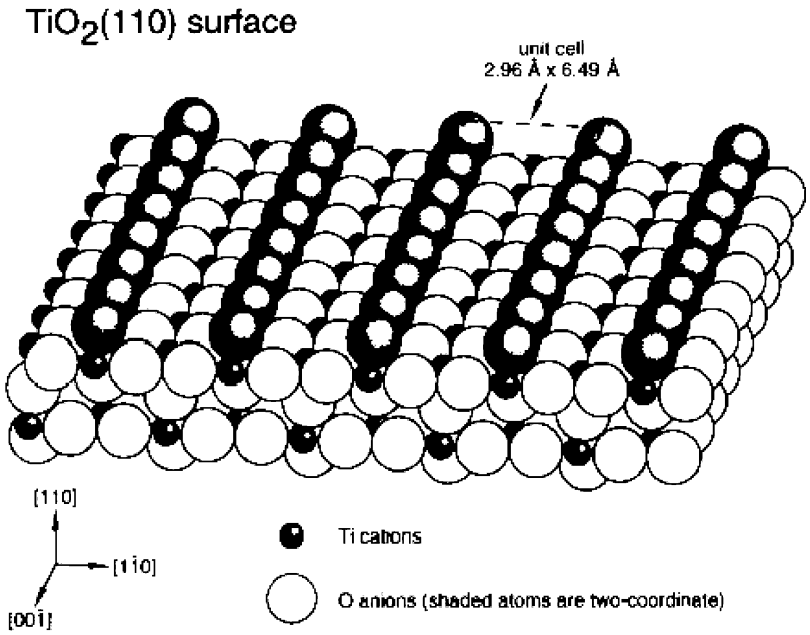

Figure 3. Schematic representation of the TiO_2 (110) surface. The surface Ti and O atoms are shown as indicated in the Figure. Reprinted from ref 41, copyright 1996, with permission from Elsevier.

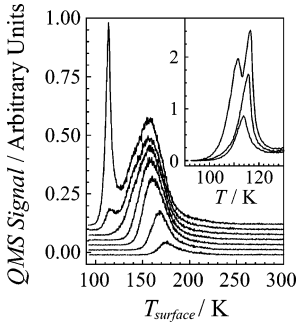

Figure 4. TPD spectra for CH_3Br from bare GaAs (110); coverages progress from 0.08, 0.23, 0.46, 0.62, 0.77, 0.93, and 1.4 ML, from bottom to top. The spectra are displaced vertically for clarity. Inset: low-temperature range of TPD spectra measured at higher coverage; coverages are 1.4, 1.9, and 2.8 ML, from bottom to top. Reprinted with permission from ref 48. Copyright 2006 American Chemical Society.

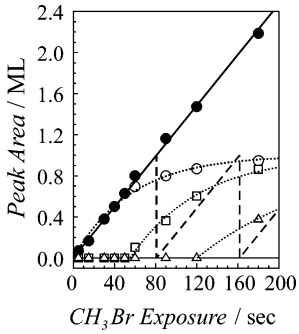

Figure 5. The integrated intensities of the desorption waves observed during the TPD of CH_3Br from bare GaAs (110): total TPD signal (●), monolayer desorption wave (○), bilayer desorption wave (□), and trilayer desorption wave (△). The solid line indicates that the total integrated intensity scales linearly with exposure. The dotted lines are guides to the eye. The linear "sawtooth" waveform (− −) illustrates ideal layer-by-layer growth and desorption. Reprinted with permission from ref 48. Copyright 2006 American Chemical Society.

molecule bound to the surface through strong electrostatic forces and with the molecules' being oriented through surface interactions.[45,46] Growth has been shown to proceed nearly stepwise, layer-by-layer, from monolayer through trilayer. The activation energy for desorption of the monolayer, E_d, has been measured to be coverage-dependent, decreasing with increasing coverage due to repulsive dipole−dipole forces among the surface-aligned molecular dipoles.[31,47] For reference, at a coverage of 0.3 monolayer (ML), a leading-edge analysis has given E_d equal to 0.53 eV, a value somewhat higher than for many physisorbed systems.

Figure 4 shows representative TPD spectra, which were collected at several values of coverage from 0.08 to 2.8 ML and with the films grown on an ∼85 K substrate.[48] Three important features[48] are apparent. First, the features corresponding to monolayer, bilayer, and trilayer desorption can be clearly distinguished. Second, the onset of growth of the bilayer desorption feature is not observed until the monolayer feature is close to saturation. Third, there is a clear shift in the position of the peak in the monolayer desorption wave to lower temperature with increasing coverage. In Figure 5, the integrated intensity[48] under the TPD curve has been decomposed (see Figure caption) into the contributions of each of the different layers in the CH_3Br film as well as the integrated intensity of all CH_3Br TPD features. The various curves are internally consistent; for example, the monolayer

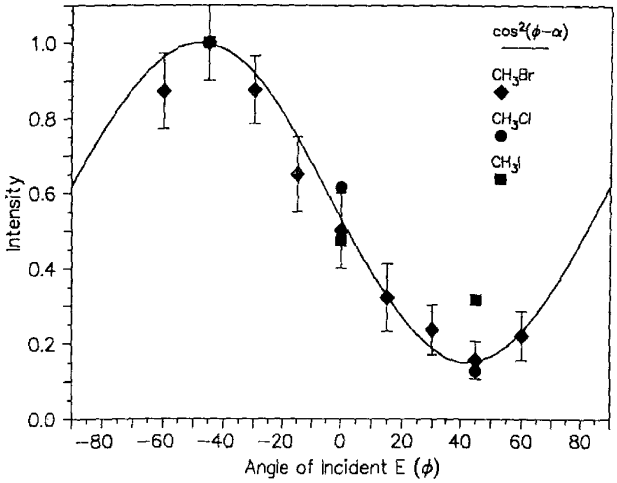

Figure 6. Plot of the variation of the surface tilt of the C−X molecular axis in 1 ML of CH_3X on GaAs (110) obtained by a NEXAFS measurement of the σ^* resonance intensity as a function of the angle of polarization of the X-ray probe beam, ϕ, with respect to surface normal. The fit to a $\cos^2(\phi - \alpha)$ curve for the methyl bromide data gives a maximum of $\phi = -48°$, implying a molecular tilt angle, α, of $-48°$, again with respect to the surface normal. Reprinted from ref 46, copyright 1995, with permission from Elsevier.

data is coincident with the total integrated curve until the onset of bilayer growth. Note also that since the total integrated curve is linear throughout the range here, the sticking coefficient is constant versus exposure. The linear "sawtooth" waveform (long-dashed line) illustrates ideal layer-by-layer growth and desorption, while the short-dashed lines indicate the successive development of the three desorption features. The sawtooth waveform is derived from the linear total integrated area curve by terminating the growth at the observed peak area value for saturation of the first monolayer and then offsetting the linear ramp by the 1-ML exposure-time equivalent for each added monolayer. This comparison with the experimental data shows that the monolayer is ∼70% complete when the bilayer begins to grow. Likewise, the bilayer is ∼70% complete when the trilayer begins to grow. This interpretation of the data shows that growth at 85 K approximates a layer-by-layer modality but is not completely ideal.

With regard to the orientation of the adsorbed molecules, several groups have examined the orientation of methyl halides on a variety of surfaces.[46,49,50] For example, in the case of CH_3Br on GaAs (110), the adsorbate surface structure has been closely examined through the use of synchrotron measurements and *ab initio* theory. In the first case, NEXAFS measurements[46] (see Figure 6) with polarized absorption for CH_3X, with X = Br, Cl, and I, were used to determine directly the orientation of the C−X bonds; these were found to be tilted at ∼45° ± 5° with respect to the surface normal. Furthermore, this direction was found to switch when a second adsorbate monolayer is added to the surface. *Ab initio* cluster calculations[51] showed that longer-range electrostatic forces between the surface and the molecule dipole set this orientation. By comparison, CH_3Br or, more generally, CH_3X molecules are known to adsorb at a coverage of ∼1 ML on metal surfaces with their molecular C−X axis perpendicular to the surface plane.[8,26,52] Note that for coverages ≪1 ML, the molecules tilt close to the surface plane.[52,53]

4. A Model System to Illustrate the Fundamentals of Reaction Dynamics on the Surfaces of Wide-Band-Gap Crystals: Alkyl Halides on GaAs (110)

4.1. Optical-Excitation to a Dissociative State of Near-Surface Molecule Fundamental Processes

Optical excitation to a dissociative state can, in the absence of surface quenching, lead to fragmentation. This process can be studied using time-of-flight mass spectrometry, which can resolve both the mass and kinetic energy of the dissociation fragments. Ideally, by studying the fragments from a surface photodissociative event, one should be able to determine if bond scission occurs with the same fragmentation pattern as it does in the gas phase and whether the fragmentation dynamics have been perturbed by surface interactions during or following bond cleavage. There are two basic questions that must be answered regarding fragmentation. First, what products does the fragmentation process yield? Second, what are the energy distributions of the photoejected fragments? In both cases, the answers are most meaningful when they are compared with gas-phase data. Since we are most interested in the basic molecule−crystal system, in this section, we will concern ourselves only with results at low coverage, where interadsorbate interactions are minimized.[54,55]

4.2 Direct Photodissociation

There are two common mechanisms for dissociation of weakly bound molecules after irradiation of the adsorbate system: direct photodissociation and electron-initiated reactions, typically dissociative electron attachment. The basic process of UV-photon-assisted bond cleavage has been carefully studied for the case of an isolated CH_3Br[56] molecule; figures that illustrate the basic process are shown in Figure 7. In this process, UV light is absorbed by the molecule, with its transition strength given by the usual quantum-mechanical overlap integral,[57] so as to undergo a vertical transition from the ground or thermally accessible ground-state vibrational levels to an excited electronic state. Direct photodissociation of methyl halides involves excitation of a lone-pair electron on the halogen atom to the repulsive continuum state, shown in Figure 7. After excitation, the methyl−bromine bond will separate, and both fragments will be ejected with suprathermal kinetic energy. Since CH_3 is by far the lightest fragment, it will receive virtually all of this kinetic energy. Notice that for the CH_3Br molecule, three excited-state, unbound, potential curves are available, which correlate to the Br atom in one of two spin−orbit states, Br and Br*. Because of their overlapping absorption spectra, both spin−orbit states of the halogen can be accessed across this UV absorption band. However, for the two prominent excimer laser wavelengths in Figure 7, predominantly ground-state Br is formed. When this molecule is then physisorbed on a GaAs (110) crystal surface, the adsorption will occur by weak physisorbed forces, and thus, the optical adsorption physics within the molecule will be, in general, only a weakly perturbed version of the gas-phase spectra.[58] Thus, it is possible to retain to first order the same physical picture as depicted in Figure 7 for direct dissociation on surfaces.

With regard to the fragmentation patterns, since the surface bonding is weak for the molecules being considered in this

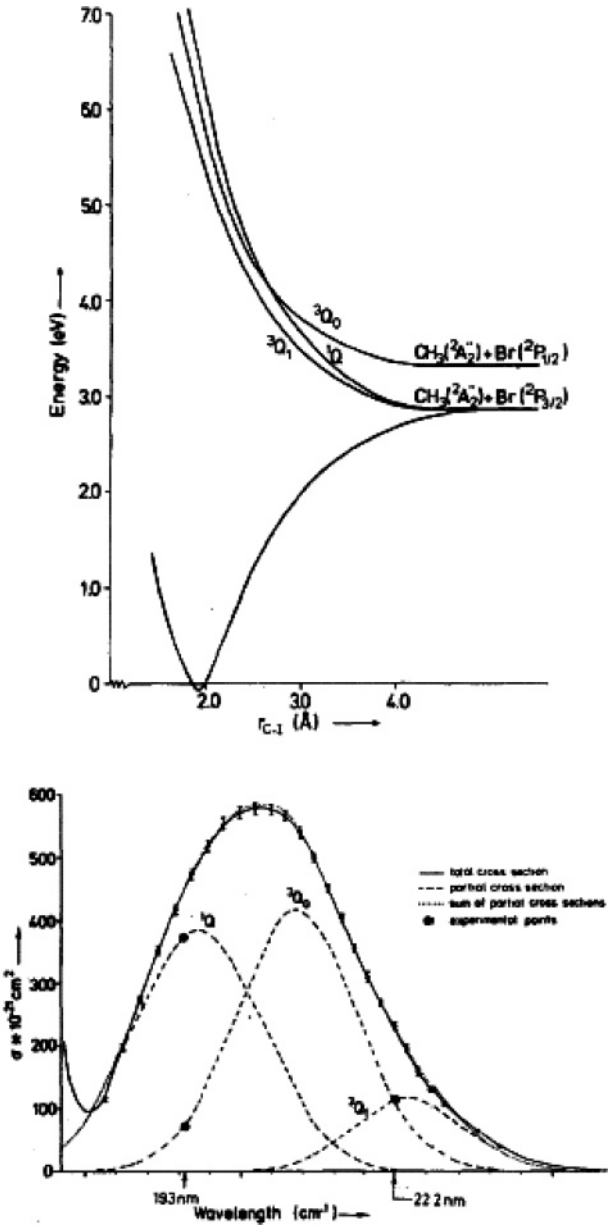

Figure 7. Potential curves (top) of CH_3Br for the first absorption continuum. The bottom panel shows the wavelength-dependent decomposition of the total cross sections of CH_3Br into partial cross sections of the ^1Q, $^3Q_0$, and $^3Q_1$ states. The partial cross sections are given by the dashed lines. The sum of these cross sections is the dotted line; the total cross section including other electronic transitions is given by the solid line. Reprinted from ref 56, copyright 1985, with permission from Elsevier.

article, it might be expected that the *fragmentation*, that is, species and energies, also would be a perturbed version of gas-phase photofragmentation. In fact, to first order, this result is generally observed. For example, in the case of CH_3Br on a wide-band gap insulator, such as single-crystal LiF, at low coverage, photodissociation at 193 nm leads to the production of CH_3 and Br radicals, just as in the gas phase.[11] However, except at the very lowest coverage, small amounts of CH_3Br are also ejected from the surface, apparently due to collisions of the hot fragments with undissociated surface-bound molecules or from quenched electronically excited CH_3Br.[59] Similar behavior is seen on other methyl halide and HX molecules. The kinetic energy of the CH_3 fragment is, to first order, that seen in the gas phase at the same wavelength, except that weak interactions

with the surface cause broadening of the observed kinetic energy.[11,60] Finally, loss of excitation energy prior to separating will prevent dissociation, as is seen, for example, on metal crystals.[4,8] This quenching process is largest for the process of resonant charge transfer across the interface.[4,61] In this process, after excitation, the electron in the excited molecular orbital is captured by transfer into an unoccupied band in the substrate, while a substrate electron tunnels in the opposite direction through the surface barrier into the photogenerated valence hole in the molecule. Excess energy is absorbed by Auger-excited electron excitation in the substrate. This process can be exceedingly fast, that is, $\sim 10^{-15}$ s,[4,8] and is thus strong for photoexcitation far above the Fermi level. Interfacial charge transfer dynamics have been studied extensively not only by ultrafast optical probing methods but also by X-ray photoemission and Auger spectroscopy.[62,63] The existence of this quenching is, thus, a major difference between the dynamics in the gas phase and that on the surface.

4.3. Tunneling of Hot Electrons into Surface Adsorbates

Dissociative electron transfer into halogenated hydrocarbons is comparatively well understood[60,64,65] for the isolated molecule. It has also recently been studied in detail using electron-beam excitation of molecules adsorbed on metal crystals, including in the presence or absence of inert spacer layers.[66] In this process, shown schematically in Figure 8 for the case appropriate to photochemical initiation, a substrate electron is excited by absorption of a photon within the substrate crystal. If the electron is given sufficient energy and is close enough to the interface to reach the interface boundary prior to any inelastic scattering event,[34] it may either tunnel through the crystal surface barrier or simply travel over this barrier; it can then be captured by the target adsorbate molecule. Note as indicated earlier in the Introduction, this process has been explored extensively for metal-crystal substrates.[8,20,67] In addition, the model shown in Figure 8 has been used in conjunction with an experimental measurement to obtain a quantitative fit for the well-studied case of electron tunneling into CH_3Br/GaAs (110); this result will be discussed in section 4.4, below.

The physics of dissociative attachment process on surfaces *after* electron capture is shown in Figure 9; it is summarized the following equation,

$$\sigma_g = \sigma_{cap} \exp(-\tau_c/\tau_a)$$

where σ_g is the cross section for dissociative attachment, σ_{cap} is the cross section for electron capture, τ_a is the anion lifetime limited by detachment to substrate, and τ_c is the time for transit from the point of electron attachment or capture to the crossing point with the neutral ground-state molecule potential curve. This equation is reminiscent of that for Menzel−Gomers−Redhead electron-stimulated desorption in the DIET process.[68] Since the full coordinates for describing the potential-energy surfaces of polyatomic molecules can be complex, it is necessary to focus only on one important coordinate and simplify the physics of the molecular separation. The quasidiatomic approximation, which has been made by Christophorou[69] and Burrow[64] and their co-workers for normal halocarbons, is valid because dissociation of these molecules is very fast and focused on the C−X bond; this assumption is sufficient for the discussion here and for

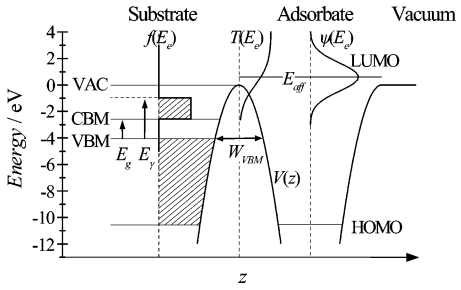

Figure 8. A schematic energy diagram of photoelectrons tunneling from a semiconductor substrate to an adsorbate molecule. Illustrated (from left to right) are the energy bands of the substrate, the interfacial barrier, and the energy levels of the adsorbate. Here, $f(E_e)$ illustrates the nascent electron distribution given an incident photon energy of E_γ, $T(E_e)$ shows qualitatively the relative probability of tunneling through barrier $V(z)$ for electrons with energy E_e, and $\psi(E_e)$ represents an affinity level of the adsorbate. Reprinted from ref 74, copyright 1998, with permission from the American Institute of Physics.

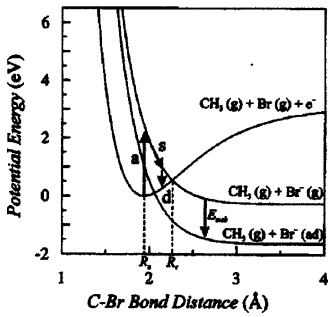

Figure 9. Potential-energy curves in the C−Br bond coordinate for the ground state of methyl bromide and for the repulsive anionic curve corresponding to the isolated gas-phase molecule as well as surface-stabilized (by energy E_{stab})CH_3Br^- ion. After electron attachment, process a, the ion propagates on the repulsive curve, process s. The anion will not dissociate if autoionization takes place before reaching R_c or point d, on the excited curve. Reprinted with permission from ref 77. Copyright 1999 American Chemical Society.

analyzing many experimental results. Note that, for a given molecule, σ_{cap} is fixed and to the very first approximation is that of the gas-phase molecule. However, τ_a is dependent on the details of the relative energetics of the surface/molecule interface as well as the density of available states in the substrate. Note also that substrate stabilization occurs through its dielectric function as well as any contribution from nearby adsorbates, through polarization (or image change) effects, to give a lowering of the final-state curve by $E_{stab} \sim 1.2$ eV, for GaAs. This stabilization reduces τ_c and, hence, increases the cross section, σ_g.

In the previous section on direct dissociation on surfaces, the importance of resonant charge transfer was discussed for the quenching of a photoexcited molecule. This process requires the presence of both an excited electron and a hole in the adsorbate molecule. In dissociative electron attachment, only an excess electron is present, since the process involves photomediated charge transfer from the substrate. As a result, quenching in this case involves simple recapture of the electron by the substrate. This process can be as fast as resonant charge transfer, and thus, one would anticipate that attachment would be fully quenched in the first monolayer prior to bond cleavage. However, back-transfer will be inhibited by loss of electron energy and stabilization in the adsorbate ion *and* a low density of states or even a band

gap in the substrate crystal. As will be shown below, this is apparently the case, since DEA is seen on the GaAs (110) surface.

4.4. Observations of CH_3Br Photofragmentation, Its Mechanisms, and Energetics

UV irradiation of a CH_3Br/GaAs (110) surface yields photofragments, which at low coverage are principally superthermal-energy CH_3 groups.[10,22] The mechanisms for production of these methyl groups have been studied carefully in terms of energies, irradiating wavelength, and coverage of the target molecule. Two of these measurements are particularly revealing. First, at a coverage of close to but somewhat greater than 1 ML, for example, say, 1.3 ML, two major energy distributions of methyl radicals have been seen.[10,22] The first, higher-energy distribution had an average energy of approximately that expected on the basis of gas-phase direct photodissociation, that is, the maximum energy of the distribution was the photon energy less than the vertical-transition energy reduced for the finite mass of the bromine atom, for example ~2.4 eV for 193 nm irradiation. This result was identical to the behavior seen also on wide-band gap alkali-halide crystals mentioned above, and thus, the methyl group with this average energy was attributable to direct photodissociation on the GaAs surface. The second distribution had a lower average energy, for example, ~1.6 eV for 193 nm irradiation. This energy was shown to be approximately that expected on the basis of dissociative electron attachment, as is explained below in this section. The second observation concerned the changes in the relative proportion of these two groups with coverage. In particular, as coverage was increased, the proportion of molecules in the faster-velocity distribution increased; conversely, if the coverage was reduced to <1 ML, this group was not seen, indicating strong quenching of direct dissociation in the first monolayer. This same behavior was seen on metal surfaces and has been attributed to resonant charge transfer, as explained above.[4,8] Conversely, as the coverage was increased, the CH_3 fragments attributable to dissociative electron attachment were seen to decrease after a coverage of a few monolayers, a result in accord with a finite mean free path of the photoelectrons. Again, this result had earlier been reported for metal-crystal substrates.[4,8,30] In the remainder of this section, we consider in more detail the behavior of the fragmentation resulting from capture of substrate electrons.

In methyl halides[69] the dissociation process is initiated by capture of an electron into the antibonding C−X σ^* orbital (LUMO). Scission of the C−X bond is the result of propagation of the molecular anionic resonance along the associated purely repulsive potential energy surface (PES), resulting in the formation of a methyl radical and a halogen anion; see Figure 9. The energetics of the fragments created by electron transfer/DEA can be used to understand the degree that this process is perturbed by the surface. For example, the energetics of the hot-electron-transfer process are illustrated by the methyl fragment translational energy of a sequence of methyl halides mentioned above. The results of this measurement are shown in Figure 10 for irradiation at 193, 248, and 351 nm.[70] The measured kinetic energies shown in Figure 10 correspond to those anticipated on the basis of changing energies for vertical attachment in these molecular species at the photon energies used here.

The energetics of the process are most clearly described by using CH_3Br as a specific model molecule; the remainder

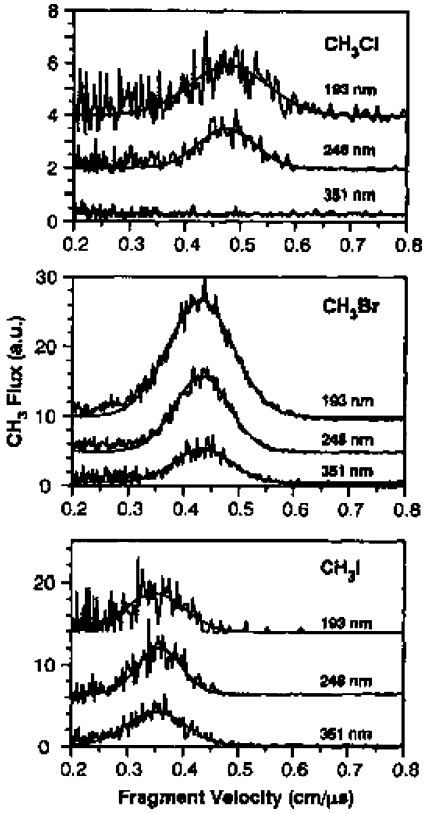

Figure 10. Time-of-flight measurements of CH_3 fragment kinetic energies after irradiation at three irradiation wavelengths from three alkyl halide species CH_3X (Br, I, Cl). Reprinted from ref 70, copyright 2006, with permission from Elsevier.

of this section will thus focus on the specific measurements and discussion for CH_3Br. Note that for this molecule, recent measurements using electron transmission spectroscopy have measured the peak in the electron-capture cross section of gas-phase CH_3Br at 2.4 eV, which is in good agreement with MS-Xα calculations of the vertical attachment energy (VAE).[71,69] At room temperature, the peak DEA cross section for CH_3Br is 10^{-18}cm^2 and occurs at an incident energy of ~0.4 eV.[72] There is a displacement of the peak of the cross section for dissociation from that for capture; this has been attributed to competition between autodetachment and dissociation, which can be treated heuristically by a survival factor.[64]

Electron-beam measurements have shown that this dissociative process is significantly perturbed for molecules adsorbed on polarizable surfaces. For example, when alkyl halides are adsorbed on single-crystal metal surfaces, with approximately a few monolayers of an inert gas spacer layer to prevent surface electron capture by the crystal, the cross section for dissociative attachment can be increased to $>10^2-10^6$ over its isolated molecule value.[66] Recent R-matrix calculations[73] have revealed that this enhancement is predominantly due to reduction in the transit time along the anionic PES from the point of ion creation to the crossing with the neutral PES for the adsorbed species. This reduction in transit time results from lowering of the LUMO by ~1 eV[26] due to polarization of the surface by the charge on the photogenerated negative ion.

The excitation-energy dependence is also an important issue in dissociative electron transfer. This dependence has implications for the minimum electron excitation energy, that is, the photon-energy threshold, necessary for initiating

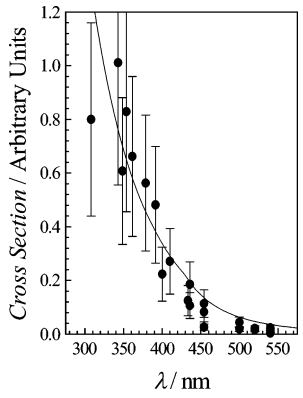

Figure 11. Measurements of the variation of the intensity of ejected methyl fragment signal resulting from photoinitiated electron attachment to this adsorbate molecule versus laser irradiation wavelength. The solid line is a fit to the tunneling model described in ref 74. Reprinted from ref 74, copyright 1998, with permission from the American Institute of Physics.

dissociation, as well for the overall energetics of the reaction fragmentation. Systematic measurements have been made on threshold energies for electrons excited above the vacuum level via the use of high-resolution electron beams.[66,73] More recently, photoexcitation studies by several groups have shown that subvacuum electrons can also be transferred into the adsorbate via tunneling through the surface barrier.[4,8,26,70,74]

The dynamics of electron transfer by the tunneling process are sketched in Figure 8. This process has been examined through measurement of the photon-energy threshold for electron-transfer dissociation of the adsorbed species using time-of-flight measurements.[74] The wavelength-dependent relative cross section of a specific dissociative pathway was then compared to a basic theoretical model, which provided a functional dependence of the tunneling process on excitation energy.[74] Note that in Figure 8, there are no details shown for the electron excitation, relaxation, or transfer process. In fact, even for a clean, well-reconstructed surface, electron dynamics are surprisingly complex. However, recent measurements using femtosecond two-photon photoemission on single-crystal metal surfaces have begun to unfold the surface dynamical processes through the use of extremely simple model systems, such as image or surface-state electron systems.[75] These studies have shown that the existence of electronic band gaps, spatial wave function overlap with surface-electron systems, etc., can play important roles in the transfer process.

Specifically, Figure 11 displays the measured variation of the ejected methyl-fragment signal, resulting from the attachment of hot electrons, as a function of the energy of the incident photons, which ranged from ~2 to 4 eV. The process was then modeled, as mentioned above, using quantum mechanical tunneling of the subvacuum electrons through the surface barrier, followed by capture into the LUMO of CH_3Br. An important element in this calculation was the assumptions regarding the incident electron energies, which follows earlier work examining DEA of O_2 on Pd (111) by Hasselbrink and co-workers.[76] The solid line in Figure 11 shows the fit of the model to the data; the parameters from the fit to the data indicate that there is a substantial lowering of the VAE with adsorption due to polarization of the semiconductor surface.[74] Thus, the surface does perturb the dissociative electron attachment process significantly. Finally, note also that as a practical matter, the existence of DEA significantly lowers the photon threshold energy for initiating bond cleavage in adsorbed molecule systems over that for isolated-molecule photoreactions.

4.5. Effects of Increases in Alkyl Chain Length (Fragment Mass) on Fragmentation Dynamics

Experiments investigating *electron*-mediated dissociation of isolated molecules have successfully used systematic variation in molecular properties as a means of elucidating the fragmentation process. For example, a systematic variation of the complexity, that is, alkyl chain length, of the adsorbate has been used to probe the dissociation fragmentation and cross section dynamics[77,78] for weakly bound linear alkyl halides. This change in the length of the hydrocarbon chain allowed the examination of the effect of the dynamic variables of the reaction, including VAE, mass of the alkyl fragment, and number of internal degrees of freedom of the adsorbate so as to understand how these quantities affect the cross section, product distribution, and efficiency of the electron-mediated chemistry.

For these experiments, three alkyl-halide adsorbates were considered: methyl bromide, ethyl bromide, and propyl bromide, all on GaAs (110), and a variety of experimental probes were employed. Temperature-programmed desorption spectroscopy was used to investigate the thermal chemistry of the adsorbed system and the surface-bound products and total photoreaction cross sections following exposure to UV light. In addition, angle-resolved TOF measurements were used to probe UV-induced fragment dynamics.[77,78] The TPD spectra showed the desorption energies for methyl bromide, ethyl bromide, and propyl bromide are 0.42, 0.45, and 0.51 eV,[77] respectively. The ~0.05 eV/CH_2 increase in energy, similar to that seen on Cu surfaces,[79] is consistent with an increase in van der Waals interaction between the adsorbate and surface with chain length.[80] The intermolecular interactions for the ethyl and propyl molecules are, thus, similar to those of CH_3Br.

TPD and TOF results show that the photochemical response of these molecules was consistent with carbon−bromine bond cleavage.[77,78] The UV-induced carbon−bromine bond cleavage resulted in ejection of a significant flux of energetic alkyl radicals from the surface. By contrast, it was found that the atomic bromine was not photoejected but remained on the surface, where it reacted with surface gallium. In addition, TPD measurements also showed a percentage of the photogenerated alkyl fragments remained intact on the surface. A certain fraction of these underwent β-hydride elimination to form ethene from ethyl and propene from propyl radicals, respectively, just prior to or during thermal desorption at ~600 K.[77] Note, however, that in the case of CH_3Br, no surface-bound hydrocarbon products were observed.

In addition, comparative energy and angle-resolved time-of-flight measurements were made on the three model systems. The angular distributions for the alkyl fragments are shown in Figure 12, using 193-nm irradiation and for detection in a plane defined by the surface normal and the [01] surface vector.[77] The time-of-flight distributions contributing to these angular distributions were deconvolved into fast- and slow-velocity groups or distributions.[77] In all cases, there was a sharp maximum for the fast species peaked at ~35−45° in the [0$\bar{1}$] direction; i.e., the fast distribution was asymmetric with respect to the surface normal; however, the

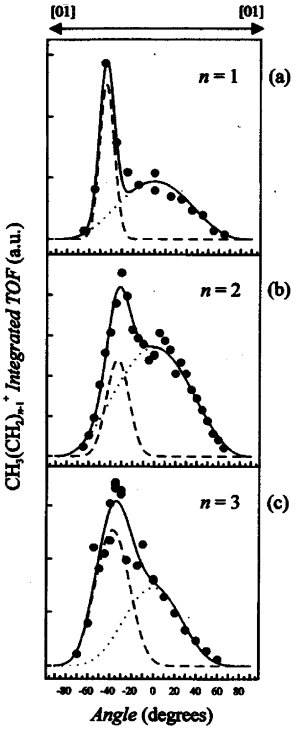

Figure 12. Comparative TOF distributions for alkyl fragments from CH_3Br, C_2H_5Br, and C_3H_7Br adsorbate monolayers (from top to bottom). The dotted and the dashed lines show the decomposition of the total TOF curve in slow and fast methyl groups, respectively. Reprinted with permission from ref 77. Copyright 1999 American Chemical Society.

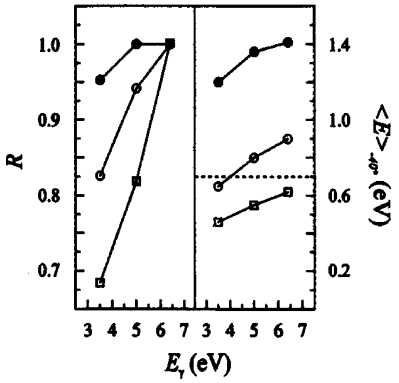

Figure 13. Plots of the anisotropy, *R*, of the angular distributions (left panel) and the measured kinetic energy (right panel) of alkyl fragments, from alkyl bromides, as a function of photon energy. The kinetic energy was measured at −40°, and methyl, ethyl, and propyl fragments are shown with a solid dot, open circle, and open square, respectively. Reprinted with permission from ref 77. Copyright 1999 American Chemical Society.

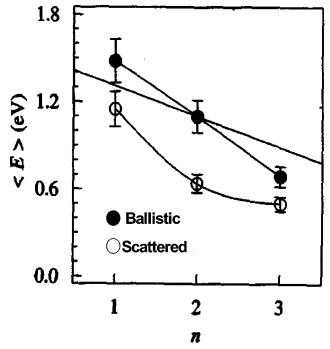

Figure 14. Graphical depiction of average fragment kinetic energy versus chain length for ejected, directly photodissociated photofragments (●) and scattered photofragments (○) from 193-nm irradiation. Reprinted with permission from ref 77. Copyright 1999 American Chemical Society.

low-energy contribution was isotropic in angle and peaked at the surface normal. The quantitative characteristics of the angular distributions associated with the two desorption channels changed considerably when the alkyl chain length and, to a lesser degree, when the excitation wavelength was varied. Since the distributions in Figure 12 were measured at 1-ML coverage, both distributions were a result of substrate-photocarrier-mediated dissociative electron attachment. The fast alkyl, anisotropic angular distributions were clearly identifiable to be a result of alkyl groups' being directly ejected from surface-oriented or "aligned" alkyl bromides; this process is discussed in detail below in section 4.7. The slower alkyl, isotropic distributions were attributed to be a result of surface scattering of the ejected alkyls; this process also will be discussed in more detail in section 4.7. Finally, note that as the chain length lengthened, an increasing number of surface-retained alkyl fragments were detected by postirradiation thermal desorption measurements.

The changes in the distributions with alkyl chain length[77] in Figure 12 appear both in the energy of the fragments and in the relative weights of the two distributions. In addition, the energies of the CH_3 fragments vary with photon energy. A plot of the ratio of the peak of the angular distribution for the fast-to-slow CH_3 fragments is shown by the quantity R in Figure 13; this quantity provides a simple metric for comparing the degree of ejected, aligned photofragments for each alkyl species. A summary of the measured kinetic energies of the alkyl desorbate fragments with chain length is also given in Figure 13.

These striking variations in the kinetic energies of the directly dissociated alkyl photofragments can be made more quantitative by a comparative plot of the kinetic energy of the alkyl fragment versus chain length, as specified by the number of carbon atoms, *n*.[77] The data from the time-of-flight measurements for the directly ejected photofragments are shown in the lower curve of Figure 14. The data show clearly a distinct flight time, or velocity, for each specific chain length. An analysis[77] has been made of the kinetic energy expected for ethyl and propyl fragments, assuming that the average energy liberated is 1.3 eV, irrespective of the chain length. This analysis indicated clearly that for propyl bromide, the measured energies were much lower than simple momentum considerations predicted. The authors of this work suggested that as chain length increased, an increasing amount of energy was channeled into internal excitation; see ref 76 for details.

4.6. Cross Section and Quenching

Khan, et al.[78] have determined the photoelectron-mediated dissociation cross sections for alkyl bromides as a function of alkyl chain length and irradiating wavelength. Their experimental approach measured the concentration of dissociated molecules versus exposure using postirradiation thermal-desorption spectrometry of target molecules remaining on the surface. The dissociation cross sections obtained in this manner are plotted in Figure 15.[78]

The trends in these data are in general agreement with observations made on dissociative electron attachment for

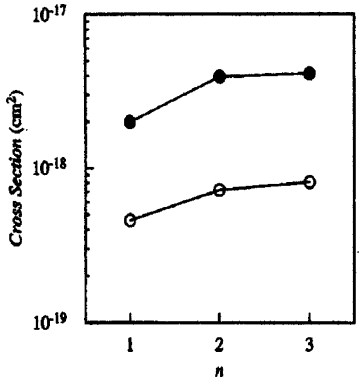

Figure 15. Measured peak cross section for electron-mediated dissociation of the three alkyl halides, CH_3Br, C_2H_5Br, and C_3H_7Br, for 1-ML coverage. See text for a discussion of the method of measurement. Reprinted from ref 78, copyright 1999, with permission from the American Institute of Physics.

gas-phase species. In particular, although it was difficult to extract *precise* absolute cross sections for electron dissociation on a per-electron basis from such surface measurements,[78] the cross sections of the adsorbed molecules could be estimated (see next paragraph) and were found to be at least an order of magnitude smaller than those measured in the gas phase. This result is surprising, given the degree of surface stabilization by the substrate crystal, and thus, it strongly suggests that the increases expected in the cross section due to stabilization of the anionic resonance via image charge and induced-adsorbate polarization interactions are compensated for by a decrease in the anion lifetime due to quenching of the excited state at the surface.

In particular, the importance of quenching was determined by making a quantitative comparison[78] of the estimated cross section for the photoinduced surface reaction to the gas-phase literature values. To make such a comparison, a simple model, assuming a flat electron-energy distribution and a Gaussian dissociative attachment line shape, was employed to extract the peak per-electron cross section for dissociative attachment in the monolayer. The peak cross sections extracted by this analysis closely parallel the reaction cross sections measured at 193 nm, suggesting that for all three molecules, at 193 nm, the photogenerated hot-electron distribution spans nearly the entire range of the adsorbate LUMO. Furthermore, the analysis implied that the interaction between the semiconductor and the adsorbed molecules significantly perturbs the dissociative attachment process: the cross sections for the physisorbed molecules are significantly smaller than those in the gas phase. Note that the interaction with the surface simultaneously lowers the LUMO and decreases the transit time of the molecular anion on the dissociative potential curve. In particular, strong charge-image charge interactions predict an ~1.2 eV lowering of the LUMO. Such a concomitant reduction in the transit time for CH_3Br from ~7 to ~1.8 fs (or less) would, all else being equal, lead to a prediction of an *increase* of a factor of 2 (or more) in the cross section based on gas-phase data for the lifetime of the molecular anion. The fact that Kahn, et al.[78] observed a *decrease* in the cross section on the surface suggested that quenching of the molecular anion is strong. In the case of methyl bromide, the data showed an estimated nearly order-of-magnitude decrease in the lifetime of the anion, from ~5.7 to ~0.6. fs, for absorbed CH_3Br.

4.7. Surface-Aligned Photofragmentation

One of the most intriguing ideas in early work on surface photodynamics was to use the surface as a template to "align" adsorbed species, an idea first proposed and realized by Polanyi and co-workers[11] for adsorbed molecules on single-crystal ionic salt substrates. This approach would allow not only the examination of the surface perturbation of the adsorbed molecule but also the investigation of the photochemistry for specific molecule/optical-field orientations. Molecule/field alignment has been used with great success in laser studies of molecular beams.[81]

There are two important criteria for such angularly oriented surface fragmentation.[22,80] First, the dissociative event must be strongly impulsive along the C−X bond. Examination of the potential-energy diagram in the case of alkyl halides, which are the model system in this discussion, for the anion formed by the attachment process or the neutral molecule, which is important in direct photodissociation, shows that each of these two final states is highly repulsive. Second, the initial orientation of the adsorbate molecules must be strongly and uniformly oriented, even in the case of a weakly adsorbed molecule. In fact, a growing body of experimental measurements has confirmed such alignment in the case of methyl halides, including those using infrared,[50] NEXAFS,[46] and STM[82] methods. In particular, the latter two methods have indicated a high degree of ordering of methyl halides on GaAs (110). In addition, *ab initio* cluster techniques[51] applied to GaAs have shown that this surface orientation derives from a combination of surface dipole forces (strong) and orbital overlap (weak) between the adsorbate and the surface.

Such ordering is confirmed by TOF experiments using the methyl halide sequence of chloride through iodide on GaAs (110). These results showed clearly that in each case when 1 ML of these three molecules was irradiated on a GaAs surface, the fragments produce a narrow, angular distribution of ~1 eV CH_3 fragments directed at angles ~40−45° from the surface normal along the $[0\bar{1}]$ direction.[70] Figure 16 shows these angular distributions for CH_3 fragments obtained by irradiation with 248-nm light. Note that GaAs has an asymmetric microfaceted surface in the [01] direction (a sketch of the surface is shown in Figure 1 above). Recall that for CH_3Br, these ~1 eV methyl fragments originated from dissociative electron attachment. If the coverage of these molecules is increased to 2 ML, the peak in the angular distribution is observed to switch to the opposite direction.[23] Additional experiments have also been done for 1-ML coverage on CdTe (110), which has an essentially identical surface structure. In that case, the hot CH_3 groups have the same angular distribution as on GaAs (110), for the same coverage of CH_3Br.[70]

As described in Section 3, TOF measurements have also been made of the variation of the angular orientation of alkyl fragments, formed by dissociative electron attachment, with the alkyl chain length for a series of alkyl halide molecules. The energetics from these measurements were described in that section. The alkyl angular distributions[77] for the series methyl, ethyl, and propyl halides for 193-nm irradiation are also shown in Figure 12. In general, the angular distributions peaked at ~35−45° from the surface normal in the $[0\bar{1}]$ direction and were focused into a relatively narrow angular range. The similarity in molecular-surface alignment for these three different chain lengths is most likely due to the importance of surface−adsorbate dipole coupling, as seen

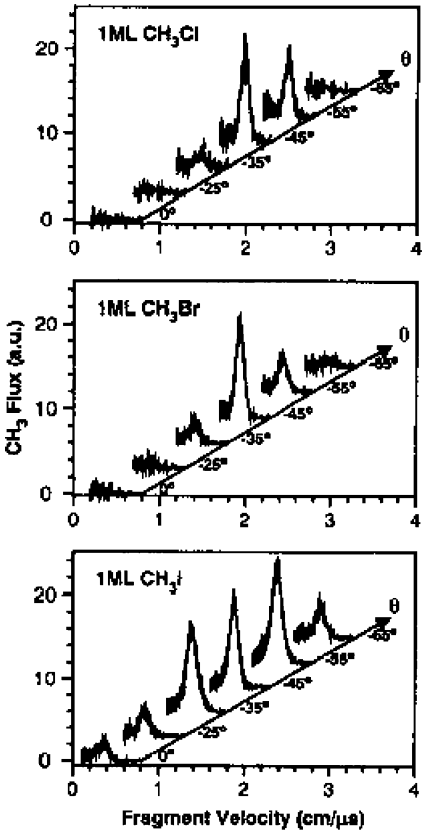

Figure 16. The angular variation of TOF spectra of CH_3 emitted as a result of hot-electron transfer for 1-ML coverage of CH_3X (X = Cl, Br, I) on GaAs (110) with 248-nm irradiation. This anisotropic fragmentation pattern is attributed to an ordered, tilted orientation (about −45°) for this coverage. Reprinted from ref 70, copyright 2006, with permission from Elsevier.

in *ab initio* studies of CH_3Br on GaAs (110).[51] In addition and as mentioned above, slower velocity distributions were also observed, which were isotropic ($\cos^n \theta$) in angular distribution. For methyl bromide, the angular distribution was dominated by directly ejected, energetic, methyl radicals at 45° (in the [01] direction) from the surface normal. For ethyl and propyl bromide, directly ejected alkyl fragments were also seen; however, scattering of species at the surface resulted in the increased importance of a slower, diffuse, $\cos^n \theta$ desorption angular distribution. These slower fragments clearly suffered collisions prior to being ejected, thereby losing memory of their predissociation-event orientation on the surface. This scattering lowered the CH_3 kinetic energies from the values seen in the directly ejected species and broadened the CH_3 TOF distribution and corresponding angular distribution. These lower-energy fragments become of increasing importance with increasing chain length and decreasing wavelength, reflecting the fact that the surface potential responsible for the scattering process becomes relatively more important with decreasing kinetic energy of the alkyl fragment. Several observations[83] suggested that these slower fragments were generated by fragments temporarily captured in the surface well. Capture of alkyl photofragments at surfaces has been reported for both metal and oxide surfaces, as well, although in some cases, these are at a coverage of >1 ML.[84,85] An important, but unresolved question is why dissociative electron attachment of some adsorbed molecules yields scattered alkyl fragments, but others have fragments with unscattered ballistic trajectories. Possibly, scattering results from a molecule with a disordered orientation, perhaps due to surface defects. The small variation in the magnitude of the slow velocity component seen among different GaAs is consistent with this explanation.

The data in Figures 12 and 13 thus show that increasing the length of the alkyl chain of adsorbed alkyl halides leads to distinct changes in the alkyl fragment angular distributions.[77] As mentioned earlier, measurements of velocity distributions of the fragments clearly demonstrated that the energy partitioned into translational motion is reduced when the number of rovibrational degrees of freedom is increased. Thus, increasing the mass and the number of internal degrees of freedom of the adsorbate dramatically alters the energetics of the ejection of the photofragments from the surface. The observed quantitative variations in the energy and angular distributions of the scattered alkyl fragments can be understood as stemming from changes in energy partitioning with alkyl chain length. Note that further studies of the width of the "direct" angular distribution could yield more subtle effects. For example, the creation of a temporary anion could lead to torques on the ion during separation due to image-charge forces. We have not examined these effects thus far.

4.8. The Role of Surface Reconstruction on the Photofragmentation Dynamics of Oriented Adsorbate Molecules

The previous section showed that molecular ordering in weakly bound adlayers results in highly angularly directed patterns of energetic fragments being ejected from a corrugated surface. In fact, many of the most dramatic effects that have been observed in photodynamics have correlated the behavior of electron-transfer, angle-resolved photofragmentation dynamics with the sites and corrugation on strongly structured surfaces.[22,46,51] A particularly dramatic example of the surface-structure-dependent change in fragment angular distributions has been seen for the case of one GaAs crystal surface when its dominant reconstruction is changed. For certain semiconductor surfaces, such changes, or "reconstruction switching," can be conveniently accomplished via small alterations of the surface composition.[86] Changing the surface from one known reconstruction to another can provide specific insight into the effect of structure and, hence, adsorption site on surface photofragmentation dynamics.

In particular, for the case of GaAs (100),[86] the surface composition and reconstruction can be changed via I-atom exposure, which removes surface As as the exposure is increased. As the surface As is removed, different reconstructed surfaces appear. The structures of the c(8 × 2) Ga-rich and the c(2 × 8) As-rich surfaces, which were used in the experiments and are sketched in Figure 17a, b, are chemical "mirror images" of each other: the lattice of one can be constructed from the other by switching As atoms for Ga atoms, and vice versa, and rotating the lattice by 90°.[87] The 2× periodicity originates from the dimer formation, and the 8× periodicity arises from a patterned arrangement of missing dimers. This surface also has some similarities in local geometrical and electronic structure with the (110)[88] surface described earlier.

Thus, in one experiment,[77,89] surface photoreaction dynamics were measured after preparing the desired reconstructed surface on GaAs (100) and dosing the surface with 1 ML of CH_3Br. Three distinct methyl-radical ejection-energy channels are then seen when the reconstruction is switched from

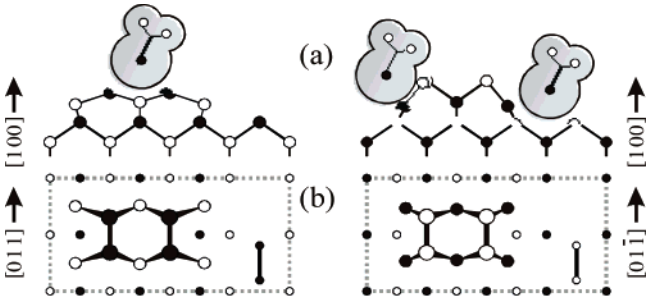

Figure 17. Side (a) and top (b) views of CH_3Br adsorbed on the (4×2) subcell of the Ga-rich c(8×2), left, and the (2×4) subcell of the As-rich c(2×8) reconstructions of GaAs (100). Solid circles represent Ga, and open circles, As. In the top view, the larger the circle, the closer the represented atom is to the surface. In b, bold vertical lines represent dimer bonds. The atomic positions were taken from the corresponding β structures in ref 89. Reprinted with permission from ref 89 (http://link.aps.org/abstract/PRL/v87/p056101), copyright 2001, the American Physical Society.

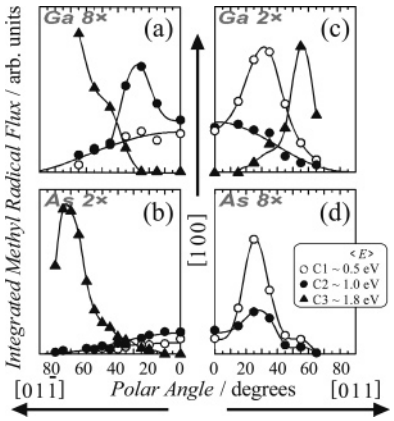

Figure 18. Results of TOF angular-distribution measurements for the three CH_3 ejection channels for both the Ga-rich (top two panels) and As-rich (bottom two panels) taken along the two principal crystallographic directions shown in the figure. Reprinted with permission from ref 89 (http://link.aps.org/abstract/PRL/v87/p056101), copyright 2001, the American Physical Society.

the Ga-rich c(8×2) to the As-rich c(2×8). Thus for the two reconstructions, the relative angular distributions and energies were different. The velocity distributions were measured from $+70°$ to $-70°$ along both the [01$\bar{1}$] and [011] directions for both the As- and Ga-rich surfaces. Each surface and direction showed clear angular dependencies that revealed a complexity in the fragmentation dynamics and that are distinct from the earlier distinctive but simple angular distributions measured on GaAs (110).[22,70] All CH_3 velocity distributions consisted of linear combinations of distributions that clustered about three distinct values: ~0.5, ~1.0, and ~1.8 eV, designed as channels C1, C2, and C3, respectively; see Figure 18. The data are displayed as a function of polar angle in four separate panels. The top two panels contain measurements made on the Ga-rich c(8×2) surface; the bottom, those made on the As-rich c(2×8).

The most striking feature of the results, shown in Figure 18, is that the reaction products are ejected with a variety of characteristic kinetic energies, each with distinct surface-reconstruction-dependent angular distributions.[89] The variations in angular distributions of the fragments reflect differing molecular orientations on the two reconstructions. The fragment angular distribution reflects the orientation of the unexcited molecule because of the impulsive nature of the bond scission following electron attachment. In this work,[89] the authors used a simple electrostatic model to show qualitatively that certain surface sites could be used to explain many of the angular dependencies in Figure 18 and their variation on the two (100) surfaces. The details of this model are given in references cited here; however, one example will illustrate the basic findings. In particular, the As-rich surface most closely parallels the (100) surface used in the work discussed above, since both the (110) and the (100) surfaces have negatively charged surface As atoms located at higher elevations relative to neighboring positively charged surface Ga atoms. Thus, one would be anticipated that the adsorption geometries on the As atom on the (100) surface would be similar to those on the (110) surface, which have been rigorously calculated using *ab initio* techniques. The calculation identified a minimum at just such a site; in addition, another minimum was found on the surface, which was only ~0.1 eV less tightly bound; see CH_3Br molecules depicted in Figure 17. Thus, multiple adsorption sites of similar binding energies were obtained; these were thought to explain the origin of the two different channels, C1 and C2 of CH_3 radicals ejected with similar angular distributions but different kinetic energies.

Finally, in this work the authors central concern was understanding the correlation of fragment angular distribution was surface structure, and thus, the portioning of fragments into specific energy channels was not extensively discussed. However, they did use their electrostatic model to estimate the degree of ion stabilization at the specific sites discussed above.[89] They found that the correlation between surface interactions and other experiments that measured the CH_3 fragment kinetic energies suggested that as the interaction of the anion resonance with the substrate increases, the kinetic energies of the fragments first increase as the ion separation time is decreased[66] and then decrease as the ion lifetime is shortened.[90] The wavelength-dependent TOF measurements for the Ga-rich surface were consistent with the affinity levels for the different channels being shifted by different amounts at different sites and revealed behavior consistent with a decrease in fragment kinetic energy with increasing stabilization energy in the strong stabilization limit.

More recently, STM measurements have been used to directly image how these oriented photoelectron-transfer reactions on semiconductor surfaces proceed at the atomic level. These experiments are distinct from the dynamics discussed above because in this case, the fragment being detected is that going toward the surface. For example, the experiment by Dobrinin, et al.[91] used UV irradiation of a 50 K, Si (111) (7×7) surface covered with 1 ML of CH_3Br. STM measurements then showed that that the UV irradiation liberated an electron from the crystal, thus allowing it to attach to CH_3Br molecules, which are bound to this Si surface in nanometer-scale circles of the Si "adatom" sites. The C−Br bond cleaved after attachment, and the bromine ion was propelled reactively into the surface to cause a distinctive change in the (7×7) reconstruction of the Si (111) surface; see Figure 19. In effect, the light pulse made very precise and local changes in surface composition of the single crystal. The authors also showed that this transformation could also be driven, as well, by electrons from an STM tip. Despite the fact that the Br is launched several angstroms above the surface, this atom is captured at the very site at which the physisorbed parent molecule was attached. The Br atom did

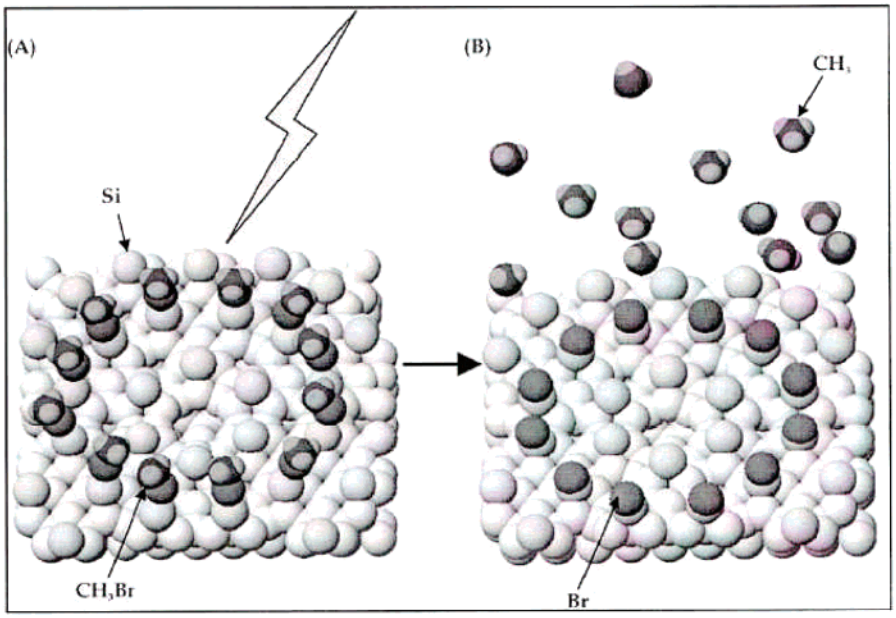

Figure 19. Representation of (A) physisorption of CH_3Br on Si (111) surface at 50 K with Br pointing down, and (B) chemisorbed Br on middle adatom positions, after surface irradiation with UV light. Reprinted from ref 91, copyright 2004, with permission from Elsevier.

not bounce or move across the surface, and once it was chemisorbed on the surface, it remained localized. Previously, laser-initiated surface chemistry[92] offered many subtle methods for patterning, and the results from these STM experiments suggest even more powerful possibilities. For example, this experiment shows that this patterning has the unexpectedly high spatial resolution of one atomic diameter!

4.9. Internal Energies

The energy-resolved studies mentioned thus far have investigated surface reactions solely though the kinetic energy of the methyl or higher-alkyl fragments; these energies have then been compared with those from the same processes in the gas phase as the photon energy or fragment mass was varied. Such measurements probe recoil effects and, indirectly, changes in internal coordinates on the surface. However, direct measurements of the vibrational degrees of freedom in the molecular fragment have also been reported in several publications; such measurements provide direct insight into the perturbation of the dynamics of the photomediated half collision via a nearby surface. In fact, with this possibility in mind, several groups have used REMPI as a probe of fragment internal excitations on wide-band-gap oxide[93−95] and metal surfaces.[96] REMPI is an ideal probe of internal excitation in photofragments and has, thus, been used successfully and exclusively to probe such states in gas-phase and molecular-beam experiments.[97] In section 5, a full discussion of CH_3 vibrational excitation on oxides is presented. More recently, several groups have also used this technique to study halide atom excitations after photoreactions on metal and oxide surfaces, as well.

Recently, state-selective REMPI[98] has been used to measure umbrella-mode excitation in CH_3 fragments during UV irradiation of CH_3I adlayers on GaAs (110). This measurement enabled comparison of the vibrational excitation in the umbrella mode following electron attachment with that after direct photodissociation bond cleavage. Specifically, the measurement used REMPI to probe the CH_3 ν_2-mode excitation after 248-nm-induced photoreaction in adsorbed CH_3I for coverage both below and above 1 ML. The results showed that both the CH_3 relative velocity and vibrational distribution depended on coverage and surface composition. For example, at high coverage, that is, ~25 ML, the velocity distribution was essentially that seen in photodissociation of the isolated molecule. By comparison, irradiation at 1-ML coverage produced a translationally and vibrationally colder distribution. These changes were attributed to the fact that direct photodissociation dominated at high coverage, whereas DEA dominated at low coverage. The reasons for this behavior are the same as those mentioned for CH_3Br in section 4.4 using TOF measurements. For intermediate coverage, both reaction channels were observed.

The most important result of this experiment[98] was that it provided a definitive correlation of the methyl vibrational distribution with its translational energy and, hence, its surface-reaction mechanism. Thus, it allowed determination of the (vibrational) internal excitation for each of the two mechanisms being examined here. The measurement showed that the methyl radicals created at 1-ML coverage, that is, from the DEA process, had a vibrational population ratio 4.4 times smaller than the same radicals created at 25 ML, that is, from the direct photodissociation process.

The measurements thus showed that electron-attachment-induced dissociation leads to CH_3 fragments with lower degrees of internal (vibrational) energy. These results thus appeared to suggest that DEA does not cause strong excitation of the CH_3 umbrella mode. However, a comparison with the behavior of the isolated molecule was not possible because there are no measurements of internal excitation in methyl or any other molecular fragments following DEA. Nonetheless, the authors of this experimental work point out that calculations of excited geometries for the negative ion suggest that one important differentiating factor between the two processes is the difference in the excited-state geometry prior to full C−I bond cleavage for the anion versus the neutral molecule. Thus, in direct photodissociation, C−I bond cleavage occurs without any significant relaxation of the CH_3I bent geometry. In contrast, during the electron-transfer

process, the nascent CH_3I^- anion could[99] undergo rearrangement to an ion−radical complex having a planar structure ($I^-{\cdot}HCH_2$) that would make the CH_3 moiety move away from its bent structure prior to C−I bond cleavage. This difference would contribute to less excitation of the CH_3 fragment in DEA, as compared to that in direct dissociation. Note that it was not possible to rule out experimentally that vibrational excitation of CH_3 was relaxed, during the attachment process, by substrate interactions. This clearly did not happen for the direct dissociation, since its vibrational distribution appears to be similar to that seen in gas-phase photodissociation. However, the fragments created by attachment do have lower translational energies, and earlier measurements[77] had shown that fragment surface translational-energy exchange does increase as the fragment translational energy is lowered.

4.10. Photoprocesses in More Strongly Adsorbed Molecular Systems: Thiols on GaAs (110)

The experiments described above have used alkyl halides as model molecular systems. They are labile to both photon- and electron-mediated bond cleavage. In addition, their large molecular dipole can lead to a well-defined molecule-surface orientation and, hence, ordered monolayers. Finally, because they are weakly molecularly adsorbed, their electron and photon interactions are in many cases found to be a perturbed version of comparable processes for the isolated molecules. It is thus of interest to examine cases in which the magnitude of this surface bonding "perturbation" is larger.

Such a study has been done with thiols, another class of molecules, which form ordered intact molecular layers. A recent study using STM and other UHV probes shows that such intact molecular layers are also formed on metal surface, that is, single-crystal gold.[100] One might expect that since their surface binding, ∼0.8 eV, to GaAs (110)[101,102] is stronger than alkyl halides (perhaps due to a weak form of hydrogen bonding[101]) by ∼50%, the coupling of the excited state with the crystal and, hence, their excited state energy quenching, as well as the interaction of fragments with the surface potential, may be different. Note also that thiol layers have served as model systems for studying processes such as interfacial electron transport.[103] In fact, the electron chemistry of surface-adsorbed thiols, primarily relatively long-chain species, such as butanethiol to hexadecanethiol, have recently been the subject of several investigations, including those with both practical and fundamental goals.[104,105] In one of these experiments,[105] thiols adsorbed on metal substrates were irradiated by an external electron beam, with the experimental results showing that dehydrogenation of the terminal methyl group was the dominant electron-induced reaction and that the cross section for this process increased with chain length.

Recently, photodynamic studies have been done on the smallest-molecule thiol system, namely, methanethiol, on GaAs (110).[102] The accompanying TPD measurements, as well as earlier work,[106] showed that the interaction between CH_3SH and the GaAs surface resulted in molecular adsorption. However, the measured adsorption energy was more than the sum of van der Waal's forces and adsorbate/dipole/surface/dipole interactions, placing this system in the interesting adsorption regime that lies between physisorption and chemisorption. In fact, some degree of electron-density sharing between the sulfur and the surface, most likely at Ga sites where the empty dangling bond may accept electron density from a sulfur lone pair, was indicated. The molecular nature of the first-monolayer adsorption meant surface photochemistry experiments could be undertaken on the CH_3SH/ GaAs (110) surface system and that the results could be sensibly compared to photoreaction dynamics of the isolated molecule.

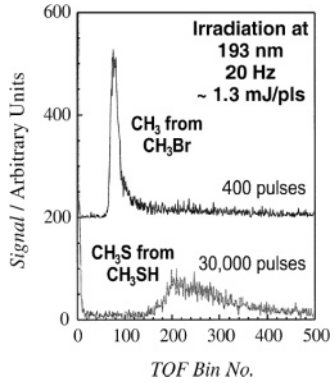

Figure 20. A comparison of TOF measurements of the products of photoinduced fragmentation of CH_3Br (upper) and CH_3SH (lower) adsorbed on GaAs (110). The products are CH_3 and CH_3S, respectively. The flux of fragments detected for fragmentation of CH_3Br is orders of magnitude higher than that for CH_3SH because the majority of the fragments in the latter case are trapped at the surface. Reprinted with permission from ref 102. Copyright 2002 American Chemical Society.

This study of the photoinduced chemistry of thiols adsorbed in monolayer quantities on the GaAs (110) surface showed important differences from that seen in gas-phase photochemistry.[102] For example, the results showed that adsorption on this semiconductor surface strongly quenched the normal gas-phase photoresponse of the molecule and altered the product branching ratio. In particular, using post-irradiation TPD measurements of the methane thiol photolysis, it was shown that the UV photoinduced reaction cross sections dropped rapidly with increasing wavelength from $\sim 2 \times 10^{-20}$ cm^2 at 193 nm to 2×10^{-21} cm^2 at 248 nm to below our detection limits at 351 nm. Note that these cross sections are ∼2 orders of magnitude less than those observed in the gas phase.[107] Furthermore, TPD and TOF measurements showed that the CH_3SH was preferentially cleaved at the S−H bond, irrespective of the wavelength of the incident light (see Figure 20). Thus, in this experiment, the photoreaction led to a trapped reactive thiolate species, which subsequently underwent a thermally activated rearrangement reaction[106] with a neighboring thiolate to evolve dimethyl sulfide. The wavelength insensitivity of the bond cleavage was distinct from that observed in the gas phase, in which a substantial change in the S−H/S−C cleavage branching ratio was earlier observed when the wavelength was tuned from 192 to 222 nm.[107] Hence, these results suggested that surface chemistry is either a greatly perturbed version of gas-phase photolysis or is due to an electron-mediated reaction. Given the stronger surface binding for thiols and, hence, the almost certain quenching of direct photon-assisted bond cleavage, the differences in photochemical response were attributed to an electron-mediated event. Thus, in this case, the surface photodynamics were still similar to that of the alkyl halides, despite stronger surface bonding. Angle-resolved measurements were also made with this surface system and showed that the angular distribution is consistent with a surface-normal-oriented molecule, that is, with the C−S bond axis oriented 90° with respect to the surface plane.

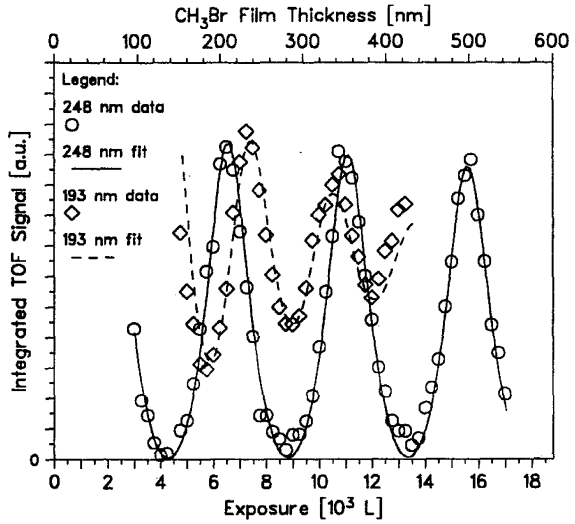

Figure 21. Integrated TOF signal flux of the direct dissociation peak in a time-of-flight mass spectrometry experiment versus overlayer thickness (or CH_3Br exposure) at 193 (○) and 248 nm (◇) irradiation wavelengths. The lines represent least-squares fits to the electromagnetic model. The s-polarized laser light impinged on the sample at a 60° incidence angle. Reprinted from ref 109, copyright 1992, with permission from the American Institute of Physics.

4.11. Surface Contouring of the Optical Field

Thus far in this review, there has been no discussion of the role of the surface in modifying the optical field of a freely propagating beam of photons.[108,109] In fact, the surface can play a major role in enhancing or diminishing this field due to either simple scattering effects or resonant interactions between elementary excitations within the substrate and the irradiating beam. Clearly, these effects are of maximum strength with a metallic substrate because of its large dielectric constant and the existence of its plasmonic response; in fact, early experiments in the exploration of laser-surface photochemistry allowed the observations of plasmon-enhanced surface reactions on metal particles.[108] Such effects can also be important for semiconducting crystals for UV surface irradiation because these crystals have a similar, metallic-like dielectric response at UV wavelengths.[110,111]

As an example of a very basic modification of an optical field and it effects on surface photoreaction dynamics, consider the photoreaction rate of surface CH_3Br, as measured by very energetic photoejected CH_3 fragments, as a function of CH_3Br overlayer coverage. The results of such an experiment[109] are shown in Figure 21. Since the coverage of the methyl bromide is heavily multilayer, the dominant photoreaction scheme in this case is direct photodissociation. The figure shows that as the coverage of CH_3Br was increased such that it had a thickness comparable to that of an optical thin film, the optical field, which took on the character of a standing wave due to reflection of the incident wave at the surface, varied sinusoidally with adsorbate thickness and, hence, reflectivity. Note that in this scheme for reaction detection, the photoelectron rate changed with the strength of the optical field at the surface, since only molecules at the surface ejected uncollided CH_3 fragments. Additionally, if the photoexcitation beam wavelength was changed, the optical field interference also changed and, with it, the near-surface optical field and, hence, the photoreaction rate.

5. Observations of Photoreaction Dynamics on Oxide Surfaces

The study of photoreaction dynamics on oxide surfaces is somewhat more recent in origin than those on metal, alkali halide, and semiconductor surfaces. Nonetheless, studies on single-crystal oxides have been extensive and have clarified the role of the crystal band gap in influencing the reaction dynamics. The study of oxides is particularly important because of the central role that these materials play in solar-energy generation, catalysis, and environmental degradation of organic molecules, all of which can involve light surface irradiation. Two of the choices of model oxides for this review, that is, TiO_2 and Fe_2O_3, are central in each of these three areas.

Oxides offer several different properties that can influence the behavior seen in the examples of semiconductor surface photoreactions described above. First, they can have extremely wide band gaps.[24,30] This band structure can present a large energy barrier to surface-bulk coupling. For example, energy transfer[4,112] from a photoexcited adsorbate via electron-hole generation can be prevented by this energy barrier to substrate excitation. Alternatively, photoexcitation of the oxide near-surface region to form excited carrier pairs for photomediated electron or hole reactions is also prevented by a wide band gap at near-UV irradiation wavelengths. In addition, because of the importance of ionic bonding[30] in oxides, their surfaces consist of ionic sites that can participate in surface−adsorbate bonding via acid−base interactions.[5,24] The electrostatic forces in this case also can "surface-align" a dipolar adsorbate molecule and, hence, lead to a well-ordered, molecular-adsorbed monolayer.

Many of the characteristics of wide-band gap oxides are shared by alkal halide salt crystals:[30] both can be insulating, with large band gaps, and have ionic surfaces. Photodynamics measurements on these surfaces have been studied extensively by Polanyi and co-workers.[27,113] Not surprisingly, then, the experiments on these surfaces have yielded many of the same insights into photoreaction energetics, mechanisms, and phenomena as those on oxides. In the discussion below, we will briefly refer to some of these alkali−salt experiments explicitly; however, the reader is referred to the many of the papers in this area in the references for complete details.[27,113]

5.1. Wide-Band-Gap Oxides

An extensive body of research on surface photodynamics has been carried out on the wide- and medium-band gap crystals of MgO and rutile TiO_2, respectively. These experiments have used many of the same experimental methods that were described above for the GaAs (110) surface and that are familiar in gas-phase photodynamics measurements. In particular, Stair and Weitz and co-workers[93−95,114−116] have investigated the photochemistry of methyl iodide on MgO (100) and TiO_2 (110) surfaces and showed that the photochemistry on these substrates is dominated by direct photodissociation. They attributed the absence of strong excited-state quenching to the relatively wide, that is, 7.8 and 3.1 eV, band gap energies of MgO (100) and TiO_2 (110), respectively. Their experiments used both REMPI and angle-resolved TOF and modulation-waveform mass spectrometry. Our discussion of this work is divided up into sections on dynamics, mechanisms, and the observations of hot-fragment reactions.

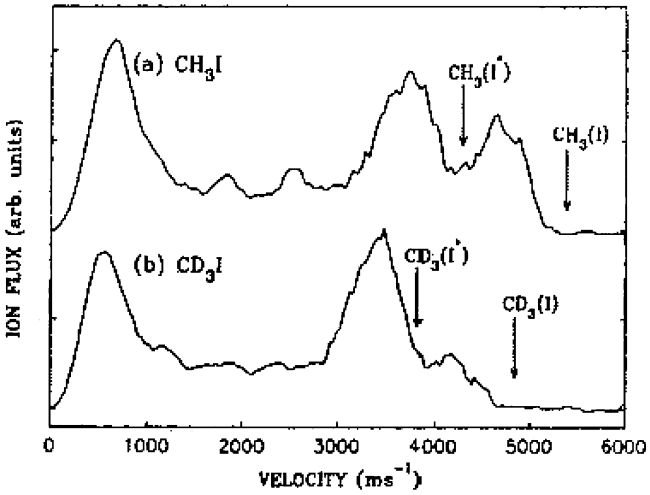

Figure 22. Flux-corrected velocity distribution of (a) CH_3 and (b) CD photofragments produced from irradiation of methyl iodide adsorbed on MgO (100) taken using REMPI at ~333 nm. The methyl(I) and methyl(I*) arrows indicate the expected velocities for methyl radicals produced in conjunction with ground (I) and spin−orbit excited (I*) state iodine. Reprinted from ref 114, copyright 1995, with permission from the American Institute of Physics.

5.1.1. Dynamics

Two particularly revealing studies[95,114] used REMPI/timed mass spectrometry to investigate the energetics and coverage dependence of the ejected methyl radicals and atomic I resulting from irradiation of CD_3I or CH_3I on each of the above two oxide surfaces. The experiments also examined the adsorbed phases for both surface systems. The results on these two surfaces were generally similar except for the low-coverage phase.

In particular, and considering the case of TiO_2 (110) first, Holbert, et al.[95] found that at low coverage, CD_3I (or CH_3I, since both were examined) adsorbed with the methyl pointed away from the surface, that is "CD_3 up", whereas for multilayers, the molecules exhibited an antiparallel alignment, that is, molecules with CD_3 up and CD_3 down adjacent to each other. The basis for this finding is described in the next paragraph.

When irradiated at one of three near UV wavelengths, for example, 257 nm, from a modulated CW' ion laser, methyl radicals were ejected from the TiO_2 surfaces. At low coverage, these fragments had superthermal velocities, corresponding to translational energies for CH_3, which were consistent with those seen in gas-phase photodissociation of CH_3I at this same wavelength. In addition, the methyl TOF signals (see Figure 22 for comparable signals on the MgO (100) surface[114]) also showed velocity subpeaks consistent with an I*/I product ratio that was identical to that seen in the case of gas-phase photodissociation. The CH_3-up molecules, which were the dominant phase at low coverage, also showed a narrow angular distribution consistent with the orientation of the molecular axis along the surface normal. This orientation also was in agreement with separate optical polarization and angle-desorption measurements.[93] Measurements of the translational energies as a function of the irradiation photon energy showed a linear variation and a magnitude that was consistent with direct photodissociation of the adsorbed molecule.[95] TOF measurements were also made at higher coverage. In this case, the methyl fragments also showed a second, lower-energy and broader-angular-width distribution, consistent with CH_3 surface scattering originating from molecules that were oriented CH_3-down. The ratio of the percentage of the methyl radicals having high-to-low energies switched from nearly unity at low coverage to ~50−50% at higher coverage;[95] this behavior is shown in Figure 23. Returning now to low-coverage experiments, post-irradiation TPD measurements showed the presence of a high concentration of surface I. This result was indicative of the iodine atoms in the parent molecule being oriented downward toward the substrate in the first monolayer. After photoinduced bond scission, the iodine was ejected toward the surface, where the flux was captured by the substrate.

REMPI measurements[95] were used to examine the internal states of the methyl radical after surface irradiation with the modulated ion laser. These experiments enabled more specific measurements of the influence the surface and other adsorbed molecules on the internal and translational states of the fragments. For example, evidence of both excited- and ground-state spin−orbit-split I atoms could be observed within the CH_3 TOF velocity groups with the REMPI probe. Lower I*/I ratios than seen in gas-phase experiments were measured at coverages from submonolayer to multilayer. This lower ratio was attributed to spin−orbit relaxation mediated by the presence of the inherent magnetic field[117] from nearby heavy I atoms in the parent molecule layer. This result is similar to that obtained and explained for the case of CH_3I on Ag.[118] The decrease in the I*/I ratio with coverage was explained as a result of the increase in packing density or concentration of parent molecules with coverage and, hence, a faster I* to I conversion during the half collision.

However, one of the most interesting results of the REMPI measurements concerned the measurement of the degree of vibrational excitation in the umbrella mode of the methyl radical. For example, at low coverage, the amount of vibrational excitation was found to be high and, in fact, nearly identical to that seen in the case of gas-phase CH_3I photodissociation, thus indicting that the surface did not significantly perturb the vibrational excitation of molecules, which were directly ejected away from the surface after direct photodissociation. The REMPI probe in this work also allowed TOF measurements to be made, and these showed that the ejected CH_3 had a bimodal velocity distribution. The translational energies obtained for the fast channel were found to be close to gas-phase photodissociation energies, as was discussed above for TOF mass spectrometry. In addition, a lower-energy CH_3 distribution (i.e., 0.6 eV lower) was also observed at higher coverage. Unlike in the case of the TOF mass spectrometry, however, the use of REMPI enabled correlation of the internal excitations with the translational energy. In particular, the vibrational distributions obtained for these two translational energy distributions were found to be different: fragments with the lower-velocity distribution showed lower vibrational excitation. This loss in translational and vibrational energy was attributed to the same collision of the nascent fragments with the surface prior that caused the loss of translational energy, which was discussed above. Similar results were found by Huang and Guo in their theoretical studies of CH_3I on LiF.[120,119]

As mentioned earlier in this section, photodynamics experiments on CH_3I were also reported using single-crystal MgO (100) substrates by Fairbrother, et al.[114] These experiments were undertaken, in part, to ascertain if carrier

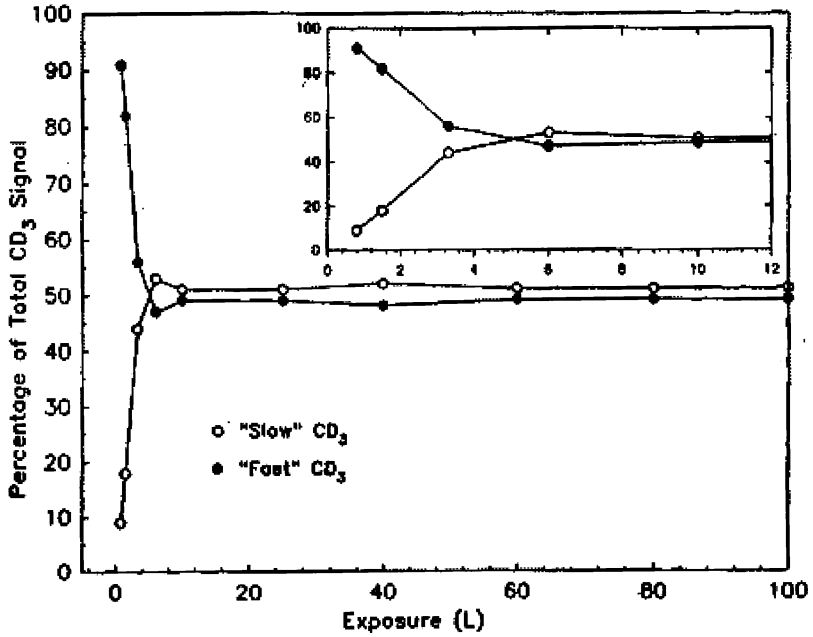

Figure 23. Velocity-resolved CD_3 photofragment yields from 257-nm irradiation of CD_3I adsorbed on TiO_2 (110) as a function of CD_3I exposure. The data points represent the fraction of the total methyl signal attributable to the integrated areas of the "slow" methyl fragments (○) and the sum of the integrated areas of the two high-velocity peaks (●). The inset is an expansion of the low exposure region. Reprinted from ref 95, copyright 1996, with permission from Elsevier.

excitation could have played any substantial role in the dynamics in the case of TiO_2, since in that case, both the band gap and the presence of surface states could in principle allow photogenerated carrier excitation. In contrast to the case of TiO_2 experiments, the use of MgO would, in the absence of surface defects, not allow substrate electron chemistry, since the band gap in this case is much wider than for TiO_2; this point is discussed in more detail in the section that follows. Such a wide band gap would not allow photoexcitation of substrate carriers or energy relaxation of a UV-excited adsorbate molecule. However, in general, the results measured for MgO were the same as for those of TiO_2. On the MgO surface, however, it was found that only the antiferroelectric, that is, an alternating dipole orientation, up and down, on the surface structure was seen, even at low coverage. Irradiation of an adsorbed layer with this structure, even at low coverage, then gave rise to high and low energies in a manner consistent with that discussed for the high-coverage TiO_2 experiments described above. In addition, in this experiment, it was possible to measure directly, using REMPI, ejected I atoms, which were believed to originate from "methyl down" molecules. These measurements enabled the atomic I kinetic energies to be determined. The results showed a high-energy tail with energies greater than those seen in gas-phase photodissociation. This higher energy was attributed to chattering enhancement involving multiple collisions between the energetic CH_3 fragment and the surface and the slowly moving, ejected I atom for CH_3-down molecules.[114,116,120] Note that the last reference just cited deals with a theoretical study on CH_3I on LiF; however, the physics is nearly identical to that on oxide surfaces. Similar results had also been observed earlier experimentally for photoreactions in CH_3Br on LiF.[59,121]

Additionally, the I/I* ratio measured for the MgO experiments was constant with coverage and higher than that seen in gas-phase dissociation; this was found to be indicative of a surface-induced relaxation of the excited I* and again, as in the case of the TiO_2 surface system, attributed to surface interactions of the I* fragment. For the case of MgO, this was attributed to transient surface trapping of iodine or heavy-atom-induced surface relaxation due to nearby CH_3I molecules. This latter effect has been reported also in two theoretical investigations.[95,122]

5.1.2. Mechanistic Aspects

Since the band gap of TiO_2 (110) is ~3.05 eV, it can act as a semiconductor at room temperature and electron−hole pairs can be created by the absorption of UV light. In addition, it is possible to dope a TiO_2 crystal and create surface band bending. The alignment of adsorbate orbitals with the band edges and the photon energy, in this case, were such that photoexcitation of substrate carriers appeared possible at the wavelengths used here, that is, generally those in the near UV. Thus, an important question arose regarding TiO_2 photochemistry on single-crystal substrates: what is the dominant cause of bond cleavage for CH_3I on this surface, electron−hole chemistry or direct photodissociation? This question was directly addressed in the measurements using modulated laser mass spectrometry[115] of the desorbed fragments. In particular, Garrett, et al.[115] used modulated CW-laser irradiation at several wavelengths and detection of CH_3 to examine how the yield varied with wavelength. Analysis of these experiments showed that the bond-cleavage cross section and wavelength dependence were such that the photoreactions could be attributable only to a photodissociation-based mechanism. The absence of substrate-mediated-carrier bond cleavage was attributed to poor spatial or energy overlap or to masking by stronger direct-dissociation channel. As a side point, it was also found that at high coverage, the photoreaction cross section was lower; this was attributed to to caging of the photoexcited parent molecule. Finally, note that irrespective of the actual measured quantities, the close similarity in the photodynamics for TiO_2 and MgO substrates (see prior section) further argues for a mechanism that does not rely on photogenerated carriers.[93,115]

5.1.3. Hot-Photofragment Reactions

The fact that on TiO_2 (110) CH_3I has both CH_3-up and -down orientation, even at low coverage, allows systematic examination of another phenomenon that differentiates the photochemistry of the low-pressure gas phase (or the isolated molecule) from that of weakly bound adsorbates; namely, that photofragment-induced secondary reactions are enabled on the surface. Note, however, that such reactions should not be present in the case of only outward-pointing molecules. With this in mind, Kim, et al.[123] used TOF mass spectrometry to investigate 257-nm irradiation of a thick CH_3I adsorbate multilayer, that is, 85 ML, on TiO_2 (110). In fact, several products were observed, which were different from those seen in gas-phase photoreactions; namely CH_4, $C_2H_6I_2$, CH_2I_2, and C_2H_5I. These were photogenerated, in part, by translationally energetic (or hot) CH_3−molecule impact reactions, which abstract H atoms from the parent molecule to form CH_4, or C_2H_6, and CH_2I. In addition, CH_2I fragments reacted in subsequent reactions with the parent molecule or other reaction fragments to form the remaining products. These processes were found to be one or two photon, depending on the number of photoproducts reacting. The measured product ratios were different on TiO_2 from those measured in separate experiments on metal surfaces, that is, Ag (111).[12,13] This difference could have reflected the fact that more energetic excitation of the molecule occurs on TiO_2 than on Ag due to the strong quenching of photoexcitation on metal surfaces. Thus, the greater excitation formed by direct photoreaction on the insulator surface would produce translationally more-energetic CH_3 than that formed by photomediated dissociative electron attachment.

5.1.4. Recent Experimental Advances

As mentioned earlier, TiO_2 (110) is in many ways the prototypical metal oxide crystal surface for experiments designed to provide an understanding of surface photochemical reactions. Despite this, it has only recently been subject to the type of UHV studies that can yield a truly precise understanding of reaction intermediates, mechanisms, and dynamics. In fact, within the last several years, there have been several significant advances in experimental techniques that promise to yield major insights into the reaction dynamics on this model crystal surface; two of these will be described here in detail. A few additional comments on other interesting related experiments will be made at the end of this section.

The first example is concerned with understanding the site-specific nature of charge transfer and trapping at TiO_2 heterogeneous photocatalytic interfaces.[124−126]

This is a difficult problem to attack under normal operating conditions due to the multiplicity of poorly defined sites and the complex environment of these interfaces. One very recent study[124] used atom-resolved STM methods, along with EELS, to probe the site-specific nature of the photochemistry at a TiO_2 (110)/adsorbed trimethylacetic acid interface. In the experiment, the surface was examined after UV (Xe arc lamp) irradiation and changes were noted as the UV exposure was increased. Through examination of the reaction as a function of surface site and energy loss using the atom-resolved probes, the authors were able to deduce the complex site-resolved processes sketched in Figure 24. In addition, they found that the photogenerated electrons were trapped at the surface cation sites. Molecular oxygen was then found to titrate these accumulated trapped electrons, thereby

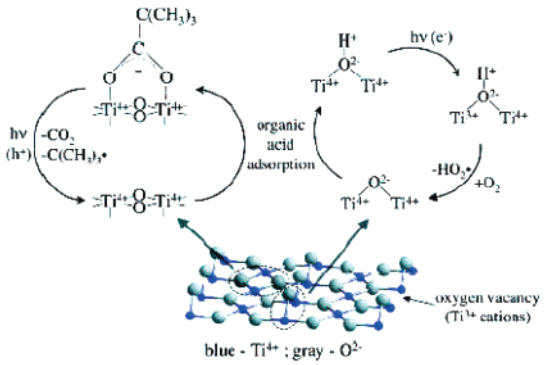

Figure 24. Reaction scheme illustrating the separate redox processes in photodecomposition of trimethyl acetic acid on a TiO_2 (110) surface, along with the sites for charge transfer and charge trapping. Reprinted with permission from ref 124. Copyright 2003 American Chemical Society.

reoxidizing the surface. Their results were also consistent with oxidation abstracting H from surface bridging OH groups.

The TiO_2 experiments in our second example were motivated by the observation that there is not a clear understanding of the detailed dynamics of electrons in the excited, surface, or interfacial states on metal oxides.[127,128] This is in part due to the lack of a convenient excited-state surface probe. However, in the past decade, the powerful probe of two-photon photoemission has been developed and found to be an effective energy- and time-resolved probe of the excited, normally unoccupied states on metal and metal−adsorbate interfaces. Thus, in the case of this experiment, Petek and co-workers have applied this technique to the problem of identifying the minority sites and their dynamics on a reduced TiO_2 (110) surface.[127] They used two-photon photoemission to determine that reduction of the surface and its attendant loss of bridging oxygen sites creates a broad continuum ~0.9 eV of occupied states below the Fermi level on this surface. In addition, on this same reduced surface, their measurements of the adsorption of molecular water suggested that this adsorption resulted in charge transfer to the Ti^{4+} sites, thus changing the surface work function, and formed a new unoccupied state 2.4 eV above E_f due to the presence of partially hydrated electrons. Subsequent experiments by the same group showed that time-resolved dynamic information on this "wet" electron could be obtained using a two-photon pump−probe approach for both the water and methyl alcohol adsorbate systems.[128−130]

Finally, and more generally speaking, STM measurements in conjunction with increasingly sophisticated STS and data analysis have been shown to allow unfolding of multistep reaction pathways along with the relevant reaction sites on the TiO_2 (110) surface. For example, STM methods have been used to unravel the dynamics of water adsorption and reaction on this surface, both on the bare surface and in the presence of surface hydroxylation.[25,131] The findings indicated that the surface chemistry is both extremely subtle and complex. Clearly, this approach can be extended so as to be used in conjunction with surface irradiation to map out photoreaction pathways on a wide variety of other metal oxide surfaces as well.

5.2. Narrow-Band-Gap Oxides

Surface photodynamics has also been investigated on oxides with much narrower-band gap (or even metallic-like)

surfaces. In these cases, the surfaces should act much like a semiconductor with a band gap of the same energy. As an example, one recent study examined the photodynamics of methyl iodide on the Fe_3O_4 (111)−(2 × 2) termination of single-crystal hematite.[132] The adsorption phases of the methyl iodine on this surface, as probed via its TPD desorption spectra, are similar to those seen on TiO_2. In the case of TiO_2, photodynamics measurements showed that, for <1-ML coverage, the CH_3I was absorbed with its molecular axis perpendicular to the surface plane and with uniform dipolar orientation with regard to the surface normal.[95] Thus, one might anticipate that the UV CH_3 dynamics could resemble either that for the semiconductor or insulator cases already discussed if the bond-cleavage mechanisms were the same.

In particular, the TOF experiments were carried out and showed two distinct CH_3 peaks, 1.6 and 0.3 eV, with the former being dominant at high coverage and the latter at low coverage. These translational energies are in accord with CH_3I photofragmentation data taken earlier on other surfaces. Thus, the fast "TOF-peak" translational energy of 1.6 eV seen in this experiment is in close agreement with typical values obtained in measurements of direct-photodissociative-ejected methyl radicals from CH_3I on GaAs surfaces using REMPI-TOF surface probing.[98] In addition, the lower-energy, that is, 0.3 eV, feature obtained on the (2 × 2)-hematite surface is also in accord with the expected properties of desorbed methyl groups following dissociative electron attachment to CH_3I by low-energy substrate photoelectrons. As in the case of GaAs semiconductor surfaces, it was found that the competition between these two bond-cleavage processes depended strongly on adsorbate coverage. Thus, the formation of high-energy fragments was found to be strongly inhibited at low adsorbate coverage. This is the behavior anticipated for a direct-photodissociation channel, since the excited state would be expected to be quenched on such a metallic-like surface for angstrom-scale molecule/substrate spacing due to resonant charge exchange with the substrate. In contrast, the high-energy peak was found to be dominant at high coverage, since in this case, the top-layer molecules are physically separated from the substrate, thus eliminating their being quenched. Finally, note these measurements here were directed heavily toward the dynamics of the methyl fragments; however, in earlier measurements on GaAs (110), it was showed that halogen fragments first-monolayer CH_3Br were only ejected toward the semiconductor surface, where they formed adsorbed halide products.[133] This same phenomena has been seen on other substrate crystals[91,94] and was assumed to occur for Fe_2O_3.

Note that the TOF data did show that a small fragmentation signal from direct dissociation was present, albeit at low intensity, even for submonolayer coverage. The authors of this work noted that, if it was assumed that the direct dissociation photolysis pathway is indeed fully quenched for the first monolayer of adsorbed methyl iodide, the presence of a detectable signal for the high-energy channel at such low, submonolayer coverage could be explained by clustering or island formation, rather than uniform layer-by-layer deposition. A similar surface phase has been reported previously in thermal desorption studies of methyl iodide Ag (111) by Zhou et al.[134] In addition, an alternate interpretation was also offered by the authors; namely, that unlike on semiconductors or metals, direct photodissociation is not fully quenched in the first monolayer due to the finite thickness, that is, <10A of the surface selvedge on Fe_2O_3 (see comments in the last paragraph in this section).

Angularly resolved measurements of the ejected methyl radical were also made on this surface system. First, and before describing these measurements, note that the TOF measurements showed that the adsorbate molecular-axis orientation of the first monolayer of CH_3I on the (2 × 2) surface was a C−I bond orientation such that the CH_3 group pointed away from the surface; this is consistent with that reported for CH_3I on TiO_2.[95] No evidence for an antiferroelectric (antiparallel) arrangement of the molecular dipoles was seen, even at higher coverage, in contrast to the results described above for TiO_2.[95] Second, the angular dependence of the ejected methyl at *each* translational energy was fitted with two distributions, including one that was highly directional and one that was more isotropic. This result indicated that a substantial portion of the methyl fragments at each energy exited normal to the surface, although the angular directionality was most striking for the high-energy (1.6 eV) peak. More specifically, the angle-resolved TOF-QMS measurements indicate that these CH_3 fragments ejected had angular distributions centered around ∼0° with respect to the surface normal. Due to the impulsive nature[135] of the dissociation, this result shows that the predominant molecular orientation in the first monolayer of adsorbed CH_3I must be normal to the crystal plane.[136] Since earlier studies of adsorbate-induced work-function changes on metallic as well as semiconductor surfaces[137] have indicated a 90° halogen-on-metal orientation, it is reasonable to expect that CH_3I is adsorbed with the electronegative iodine oriented toward the uncapped surface Fe atom on this (2 × 2) surface. The more isotropic angular component seen for each energy class was attributed to elastic, surface-scattering events. In addition, the fact that the larger angular lobe was measured for the *lower-energy* (0.3 eV) electron-mediated fragments was consistent with the results mentioned earlier in conjunction with measurements of the wavelength dependence of the photofragmentation dynamics of alkyl halides having different chain lengths. In particular, these studies showed[77] that as the fragment energy became lower, the directionality of the ejected alkyl ligands degraded. This behavior was attributed to the fact that for lower fragment energies, the importance of fragment-surface interactions increased.

Finally, the dynamic behavior observed with this substrate was consistent with a substrate crystal having the electronic properties of the natural hematite single crystal. Specifically, the incident-photon energy of 248 nm (5.0 eV) used in these experiments exceeds the 2.2 eV band gap of the bulk, single-crystal hematite, α-Fe_2O_3 (0001) allowing excitation of hot carriers. As discussed in section 4.3, depending on the magnitude of the surface barrier, such carriers can tunnel into the unoccupied molecular orbitals of the adsorbed molecule. Note also that adsorption of polar molecules such as CH_3I would increase this photoelectron flux since adsorption of methyl halides is known to lower the work function of certain substrate crystals.[136,138] Since the present experiments were performed on the "metallic" (2 × 2) *surface*, some degree of quenching of the directly photoexcited species by resonant charge exchange would occur as on single-crystal metals. In particular, magnetite is generally described in the literature as having "metallic" conductivity,[139] while a more quantitative calculation gives a band gap of no more than 0.2 eV for temperatures above the Verwey transition in Fe_3O_4.

6. Summary and Perspective

The stimulation of surface reactions by light is a basic chemical physics phenomenon that is important for a large number of real-world applications and processes. The review here focuses exclusively on its most fundamental aspects by emphasizing reaction dynamics. It also limits the discussion to substrate crystals with a finite band gap, that is, a semiconductor or metal oxide. Such a finite band gap inhibits or modifies the flow of any photogenerated carriers across the adsorbate/crystal interface. Finally, the adsorbate systems discussed in this review are limited to the case of relatively weakly adsorbed molecules; this assumption allows one to compare the photoreaction event, at least in the first approximation, to related processes for the isolated molecule.

This approach to understanding surface photodynamics allows one to see clearly that a surface alters the isolated-molecule chemical response in several major and distinct ways. First, the surface may "align" an adsorbate molecule and, thus, direct the trajectory of photofragments into specific spatial and angular coordinates. In practice, this process may inhibit hot-fragment reactions on the surface simply by directing fragments away from other adsorbate molecules. More subtle effects are possible; for example, a fixed orientation in conjunction with a polarized laser beam may allow only one specific molecular transition to occur due to the directional nature of molecule transition dipole moments.[93] Second, the surface may provide a source of low-energy photoelectrons that can be captured by adsorbate molecules after tunneling through or over (by photoemission) the substrate surface barrier. In practice, this process can greatly enhance (or even allow) a reaction rate on the surface over its value in the gas or liquid phase. Third and conversely, a nearby surface can quench a photoreaction if resonant charge transfer or simply charge transfer is energetically allowed for the photoexcited adsorbate molecule or negative ion, respectively. Quenching is most clearly seen in the case of direct UV excitation to a repulsive state in the case of molecules directly adsorbed on the surface of a metallic or small-band-gap substrate. The results given above show that dissociative electron attachment is also quenched, but not completely so. Fourth, a surface can also modify the local optical electric field due to the crystal dielectric response. In some cases, such as metallic nanospheres, this can lead to optical field enhancement, whereas in others, such as a flat surface, destructive interference occurs. Both enhancement and reduction affect the rate of any optically controlled photoreactions.

What are emerging areas for photodynamics studies, or in other words, what still needs to be learned? One important area is to obtain an atomic-level understanding of the interaction of energetic or hot photofragments with a bare surface. Recent work using STM[29,91,140] measurements (see the description in section 4.8) shows a very powerful experimental path to reaching this goal. A second emerging area is the investigation of nonadiabatic effects involving highly internally excited photofragments. For example, recent work by Wodtke, Auerbach, and co-workers[141] on the interaction of highly vibrationally excited diatomics with metal surfaces has indicated that nonadiabatic effects at surfaces can be extremely important. Finally, a third direction or challenge is the utilization of a specific photodynamics effects or phenomenon to accomplish a new surface modification procedure. For example, it has been shown that surface photoreactions involving CH_3Br result in selective bromination of certain group III−V semiconductor surface or group IV surface sites.[89] Such a selective reaction can be employed to alter the surface reconstruction or passivate surface sites. An exciting challenge is then to determine if other photoreaction processes achieve other even more subtle or powerful effects.

7. Acknowledgment

The insights provided in this paper on reaction dynamics have benefited from numerous colleagues of the author at Columbia including, most particularly, Drs. Q.-Y. Yang, N. Camillone, K. Khan, P. Lasky, and P.-H. Lu as well as Profs. George Flynn and Richard Bersohn. G. Totir and G. Le contributed discussions and comments on TOF experiments on Fe_2O_3 surfaces. In addition, comments on surface dynamics by Jim Cowin, and Steve Joyce and Kaveh Adib were important for understanding TOF data and Fe_2O_3 surfaces, respectively. Finally, the author thanks Maria Reftelis for skilled assistance in the preparation of the manuscript. The preparation of this article was supported by the DOE BES Chemical Science Division under Project No. DE-FG02-90ER14104.

8. Note Added after ASAP Publication

This review was published on the Web on September 26, 2006. Minor changes were made to the caption of Figure 7, and the review was reposted on the Web on October 2, 2006.

9. References

(1) Serpone, N., Pelizzetti, E., Eds. *Photocatalysis—Fundamentals and Application*; Wiley-Interscience: New York, 1989.
(2) Hoffman, M. R.; Martin, S. T.; Choi, W.; Bahnemann, D. W. *Chem. Rev.* **1995**, *95*, 69.
(3) Graetzel, M., Ed. *Energy Resources through Photochemistry and Catalysis*; Academic: New, York, 1983. Norris, J. R., Jr., Meisel, D., Eds.; *Photochemical Energy Conversion*; Elsevier: New York, 1989.
(4) Zhou, X. L.; Zhu, X. Y.; White, J. M. *Surf. Sci. Rep.* **1991**, *13*, 76.
(5) Lin, M. C.; Ertl, G. *Annu. Rev. Phys. Chem.* **1986**, *37*, 587.
(6) Linsebigler, A. L.; Lu, G.; Yates, J. T. *Chem. Rev.* **1995**, 95, *735*.
(7) Fox, M. A.; Dulay, M. T. *Chem. Rev.* **1993**, *93*, 3, *341*.
(8) Marsh, E. P.; Gilton, T. L.; Meier, W.; Tabares, F. L.; Schneider, M. R.; Cowin, J. P. *Phys. Rev. Lett.* **1988**, *61*, 2725; *J. Chem. Phys.* **1990**, *92*, 2004.
(9) Ukraintsev, V.; Long, T. J.; Gowl, T.; Harrison, I. *J. Chem. Phys.* **1992**, *96*, 9114.
(10) Yang, Q. Y.; Schwartz, W. N.; Osgood, R. M., Jr. *J. Chem. Phys.* **1993**, *93*, 1008.
(11) Cowin, J. P.; Harrison, I.; Polanyi, J. C.; Segner, J.; Stanners, C. D.; Young, P. A. *J. Phys. Chem.* **1984**, *88*, 6100.
(12) Coon, S. R.; Myli, K. B.; Grassian, V. H. *J. Phys. Chem.* **1995**, *99*, 16416.
(13) Zhou, X. L.; White, J. M. *Surf. Sci.* **1991**, *241*, 270.
(14) Gadzuk, J. W. *Annu. Rev. Phys. Chem.* **1988**, *39*, 395.
(15) Hanley, L.; Guo, X.; Yates, J. *J. Chem. Phys.* **1989**, *91*, 7220.
(16) Wolf, M.; Hasselbrink, E.; White, J. M.; Ertl, G. *J. Chem. Phys.* **1990**, *93*, 5327.
(17) Zhu, X. Y.; White, J. M.; Wolf, M.; Hasselbrink, E.; Ertl, G. *J. Phys. Chem.* **1991**, *95*, 893.
(18) Tolk, N.; Traum, M.; Tully, J. C.; Madey, J. *Desorption Induced by Electronic Transitions*; Diet 1, Springer Series in Chemical Physics; Springer: Heidelberg, 1983; Vol 24.
(19) Prybyla, J. A.; Heinz, T. F.; Misewich, J. A.; Loy, M. M. T.; Glownia, J. H. *Phys. Rev. Lett.* **1990**, *64*, 1537.
(20) Gadzuk, J. W.; Richter, L. J.; Buntin, S. A.; King, D. S.; Cavanagh, R. R. *Surf. Sci.* **1990**, *235*, 317.
(21) Richter, L. J.; Cavanagh, R. R. *Prog. Surf. Sci.* **1992**, *39*, 155.
(22) Yang, Q. Y.; Schwarz, W. N.; Lasky, P. J.; Hood, S. C.; Loo, N. L.; Osgood, R. M., Jr. *Phys. Rev. Lett.* **1994**, *72*, 3068.
(23) Lasky, P. J.; Lu, P. H.; Wang, X. Y.; Bent, B. E.; Stevens, P. A.; Osgood, R. M., Jr. *Surf. Sci.* **1995**, *336*, 140.

(24) Henrich, V. E.; Cox, P. A. *The Surface Science of Metal Oxides*; Cambridge University Press: Cambridge, 1994.
(25) Diebold, U. *Surf. Sci. Rep.* **2003**, *48*, 53.
(26) Ukraintsev, V.; Long, T. J.; Harrison, I. *J. Chem. Phys.* **1992**, *96*, 3957.
(27) Bourdon, E. B.; Cho, C.-C.; Das, P.; Polanyi, J. C.; Stanners, C. D. *J. Phys. Chem.* **1991**, *95*, 1361.
(28) Chuang, T. J. *Surf. Sci.* **1986**, *78*, 763. Kawai, T.; Sakata, T. *Chem. Phys. Lett.* **1980**, *69*, 33.
(29) Dobrin, S.; Harikumar, K. R.; Polanyi, J. C. *Surf. Sci.* **2004**, *561*, 11.
(30) Zangwill, A. *Physics of Surfaces*; Cambridge University: Cambridge, 1988.
(31) Somorjai, G. *Principles of Surface Chemistry*; Prentice Hall: Englewood Cliffs, NJ, 1972.
(32) LaFemina, J. P. *Surf. Sci. Rep.* **1992**, *16*, 138.
(33) Duke, C. B.; Wang, Y. R. *J. Vac. Sci. Technol.* **1988**, *86*, 1440.
(34) Haight, R.; Silverman, J. A. *Phys. Rev. Lett.* **1989**, *62*, 815.
(35) Myneni, S. C. B.; Tokunaga, T. K.; Brown, G. E. *Science* **1997**, *278*, 1106; Brown, G. E.; Henrich, V. E.; Casey, W. H.; Clark, D. L.; Eggleston, C.; Felmy, A.; Goodman, D. W.; Gratzel, M.; Maciel, G.; McCarthy, M. I.; Nealson, K. H.; Sverjensky, D. A.; Toney, M. F.; Zachara, J. M. *Chem. Rev.* **1999**, *99*, 77.
(36) Peden, C. H. F.; Herman, G. S.; Ismagilov, I. Z.; Kay, B. D.; Henderson, M. A.; Kim, Y. J.; Chambers, S. A. *Catal. Today* **1999**, *51*, 513.
(37) Adib, K.; Camillone, N., III; Fitts, J. P.; Rim, K. T.; Flynn, G. W.; Joyce, S. A.; Osgood, R. M., Jr. *Surf. Sci.* **2002**, *497*, 127. Camillone, N., III; Adib, K.; Fitts, J. P.; Rim, K. T.; Flynn, G. W.; Joyce, S. A.; Osgood, R. M., Jr. *Surf. Sci.* **2002**, *511*, 267. Adib, K.; Totir, G. G.; Fitts, J. P.; Rim, K. T.; Mueller, T.; Flynn, G. W.; Joyce, S. A.; Osgood, R. M., Jr. *Surf. Sci.* **2003**, *537*, 191. Adib, K.; Mullins, D. R.; Totir, G.; Camillone, N., III; Fitts, J. P.; Rim, K. T.; Flynn, G. W.; Osgood, R. M., Jr. *Surf. Sci.* **2003**, *524*, 113.
(38) Condon, N. G.; Leibsle, F. M.; Lennie, A. R.; Murray, P. W.; Parker, T. M.; Vaughan, D. J.; Thornton, G. *Surf. Sci.* **1998**, *397*, 278; Condon, N. G.; Leibsle, F. M.; Parker, T.; Lennie, A. R.; Vaughan, D. J.; Thornton, G. *Phys. Rev. B* **1997**, *55*, 15885.
(39) Lad, R. J.; Henrich, V. E. *Surf. Sci.* **1998**, *193*, 81.
(40) Joseph, Y.; Kuhrs, C.; Ranke, W.; Ritter, M.; Weiss, W. *Chem. Phys. Lett.* **1999**, *314*, 195
(41) Henderson, M. A. *Surf. Sci.* **1996**, *355*, 151.
(42) Herman, G.; Dohnalek, Z.; Ruzycki, N.; Diebold, U. *J. Chem. Phys. B* **2003**, *107*, 2788.
(43) Yagi, E.; Hasiguti, R.; Aono, M. *Phys. Rev. B* **1996**, *54*, 7945.
(44) Henderson, M. A.; Epling, W. S.; Peden, C. H. F.; Perkins, C. L. *J. Phys. Chem. B* **2003**, *107*, 53. Perkins, C. L.; Henderson, M. A. *J. Phys. Chem. B* **2001**, *105*, 3856. Henderson, M. A.; White, J. M.; Uetsuka, H.; Onishi, H. *J. Am. Chem. Soc.* **2003**, *125*, 14974.
(45) Lu, P. H.; Lasky, P. J.; Yang, Q. Y.; Wang, Y. B.; Osgood, R. M., Jr. *J. Chem. Phys.* **1994**, *101*, 10145.
(46) Lasky, P. J.; Lu, P. H.; Yang, M. X.; Osgood, R. M., Jr.; Bent, B. E.; Stevens, P. A. *Surf. Sci.* **1995**, *336*, 140.
(47) Maschhoff, B. L.; Cowin, J. P. *J. Chem. Phys.* **1994**, *101*, 8138.
(48) Camillone, N., III; Pak, T. R.; Adib, K.; Osgood, R. M., Jr. *J. Phys. Chem. B* **2006**, *110*, 11334.
(49) Robinson, G. N.; Camillone, N., III; Rowntree, P. A.; Liu, G. Y.; Wang, J.; Scoles, G. *J. Chem. Phys.* **1992**, *96*, 9212.
(50) Garrett, S. J.; Heyd, D. V.; Polanyi, J. C. *J. Chem. Phys.* **1997**, *106*, 7834.
(51) Black, S.; Lu, P. E.; Black, S.; Friesner, R.; Lu, P. H.; Osgood, R. M., Jr. *Surf. Sci.* **1997**, *382*, 154.
(52) Henderson, M. A.; Mitchell, G. E.; White, J. M. *Surf. Sci.* **1991**, *248*, 279.
(53) Henderson, M. A.; Mitchell, G. E.; White, J. M. *Surf. Sci.* **1987**, *184*, *L*325. Zaera, F.; Hoffmann, H.; Griffiths, P. R. J. *Electron Spectrosc. Relat. Phenom.* **1990**, *54*, 405. Fan, J. F.; Trenary, M. *Langmuir* **1994**, *10*, 3649. French, C.; Harrison, I. *Surf. Sci.* **1997**, *387*, 11.
(54) Cowin, J. P.; Auerbach, D. J.; Becker, C.; Wharton, L. *Surf. Sci.* **1978**, *78*, 545.
(55) Chuang, T. J. *Surf. Sci.* **1986**, *78*, 763. Kawai, T.; Sakata, T. *Chem. Phys. Lett.* **1980**, *69*, 33. Bourdon, E. B. D.; Domen, K.; Chuang, T. J. *Phys. Rev. Lett.* **1987**, *59*, 1484. Chuang, T. J.; Domen, K. *J. Vac. Sci. Technol. B* **1989**, *7*, 1200.
(56) Van Veen, G. N. A.; Baller, T.; De Vries, A. E. *Chem. Phys.* **1985**, *92*, 59.
(57) Hertzberg, G, *Spectra of Diatomic Molecules*; Van Nostrand: New York, 1950. Hertzberg, G. *Electronic Spectra and Electronic Structure of Polyatomic Molecules*; Van Norstrand: New York, 1966.
(58) Chen, C. J.; Osgood, R. M., Jr. *Chem. Phys. Lett.* **1983**, *98*, 363.
(59) Tabares, F. L.; Marsh, E. P.; Bach, G. A.; Cowin, J. P. *J. Chem. Phys.* **1987**, *86*, 738.
(60) Marsh, E. P.; Gilton, T. L.; Meier, W.; Tabares, F. L.; Schneider, M. R.; Cowin, J. P. *Phys. Rev. Lett.* **1988**, *61*, 2725. Marsh, E. P.; Tabares, F. L.; Schneider, M. R.; Gilton, T. L.; Meier, W.; Cowin, J. P. *J. Chem. Phys.* **1990**, *92*, 2004.
(61) Lang, N. D.; Williams, A. R.; Himpsel, F. J.; Reihl, B.; Eastman, D. E. *Phys. Rev. B* **1982**, *26*, 1728. Persson, B. N.; Avouris, P. *J. Chem. Phys.* **1983**, *79*, 5156.
(62) Wurth, W.; Menzel, D. **2000**, *251*, 141.
(63) Bruewiler, P. A.; Karis, O.; Maertensson, *Rev. Mod. Phys.* **2002**, *74*, 7003.
(64) Pearl, D. M.; Burrow, P. D. *J. Chem. Phys.* **1994**, *101*, 2940. Pearl, D. M.; Burrow, P. D.; Fabrikant, I. I.; Gallup, G. A. *J. Chem. Phys.* **1995**, *102*, 2737.
(65) Christophorou, L. G., Ed. *Electron−Molecule Interactions and Their Applications*; Academic Press: New York, 1984.
(66) Ayotte, P.; Gamache, J.; Bass, A. D.; Fabrikant, I. I.; Sanche, L. *J. Chem. Phys.* **1997**, *106*, 749.
(67) Cho, C.-C.; Collings, B. A.; Hammer, R. E.; Polanyi, J. C.; Stanners, C. D.; Wang, J. H.; Xu, G.-Q. *J. Phys. Chem.* **1989**, *93*, 7761. Dixon-Warren, St. J.; Jensen, E. T.; Polanyi, J. C. *Phys. Rev. Lett.* **1992**, *67*, 2395. Dixon-Warren, St. J.; Jensen, E. T.; Polanyi, J. C. *J. Chem. Phys.* **1992**, *98*, 5938. Dixon-Warren, St. J.; Heyd, D. V.; Jensen, E. T.; Polanyi, J. C. *J. Chem. Phys.* **1992**, *98*, 5954.
(68) Menzel, D.; Gomer, R. *J. Chem. Phys.* **1964**, *41*, 3311. Redhead, P. A. *Can. J. Phys.* **1964**, *42*, 886.
(69) Christophorou, L. G.; Carter, J. G.; Collins, P. M.; Christodoulides, A. A. *J. Chem. Phys.* **1970**, *54*, 4706.
(70) Lu, P. H.; Lasky, P. J.; Yang, Q. Y.; Osgood, R. M., Jr. *Chem. Phys.* **2006**, *205*, 143.
(71) Modelli, A.; Scagnolari, F.; Distefano, G.; Jones, D.; Guerra, M. *J. Chem. Phys.* **1992**, *96*, 2061.
(72) Datskos, P. G.; Christophorou, L. G.; Carter, J. G. *J. Chem. Phys.* **1992**, *97*, 9031.
(73) Sanche, L.; Bass, A. D.; Ayotte, P.; Fabrikant, I. I. *Phys. Rev. Lett.* **1995**, *75*, 3568.
(74) Camillone, N., III; Khan, K. A.; Lasky, P. J.; Wu, L.; Moryl, J. E.; Osgood, R. M., Jr. *J. Chem. Phys.* **1998**, *109*, 8045.
(75) Fauster, T.; Steinmann, W. In *Electromagnetic Waves*: *Recent Development in Research*; Halevi, P. Ed.; North-Holland: Amsterdam, 1995; Vol. 2. Osgood, R. M., Jr.; Petek, H.; Ogawa, S. *Surf. Sci.* **1997**, *56*, 238. Osgood, R. M., Jr.; Wang, X. In *Solid State Physics*; Ehrenreich, H., Spaepen, F., Eds.; Academic Press: Boston, 1998. Haight, R. *Surf. Sci. Rep.* **1995**, *21*, 275.
(76) Weik, F.; de Meijere, A.; Hasselbrink, E. *J. Chem. Phys.* **1993**, 99, 682.
(77) Khan, K. A.; Camillone, N., III; Osgood, R. M., Jr. *J. Phys. Chem. B* **1999**, *103*, 5530.
(78) Khan, K. A.; Camillone, N., III; Osgood, R. M., Jr. *J. Chem. Phys.* **1999**, *110*, 10526.
(79) Lin, J. L.; Bent, B. E. *J. Phys. Chem.* **1992**, *96*, 8529.
(80) Salem, L. *J. Chem. Phys.* **1962**, *37*, 2100. Camillone, N., III. Ph.D. Dissertation, Princeton University, 1994. Nuzzo, R. G.; Dubois, L. H.; Allara, D. L. *J. Am. Chem. Soc.* **1990**, *112*, 558. Zheng, D. L.; Gellman, A. J. *J. Phys. Chem.* **1991**, *95*, 7433.
(81) Parker, D. H.; Bernstein, R. B. *Annu. Rev. Phys. Chem.* **1989**, *40*, 561.
(82) Harrison, I. Unpublished results.
(83) Khan, K. A.; Moryl, J. E.; Slater, D. A.; Lasky, P. J.; Osgood, R. M., Jr. *J. Phys. Chem. B* **1997**, *101*, 9077.
(84) Zhou, X. L.; White, J. M. *Surf. Sci.* **1991**, *241*, 244; **1991**, *241*, 259.
(85) Nishimura, S. Y.; Aldrich, D. N.; Hoerth, M. T.; Ralston, C. S.; Tro, N. S. *J. Phys. Chem. B* **1999**, *103*, 9717.
(86) Varenkamp, M. C.; Hakansson, J.; Kanski, D. K. Shuh; Bjorkqvist, M.; Gothelid, M.; Simpson, W. C.; Karlsson, U. O.; Yarmoff, J. A. *Phys. Rev. B* **1996**, *53* (3), 2101. Khan, K. A.; Camillone, N., III; Yarmoff, J. A.; Osgood, R. M., Jr. *Surf. Sci.* **2000**, *458*, 53.
(87) (a) Northrup, J. E.; Froyen, S. *Phys. Rev. Lett.* **1993**, *71*, 2276. (b) Northrup, J. E.; Froyen, S. *Mater. Sci. Eng., B* **1995**, *30*, 81. (c) Schmidt, W. G.; Bechstedt, F. *Surf. Sci.* **1996**, *360*, L473.
(88) Mailhiot, C.; Duke, C. B.; Chadi, D. J. *Surf. Sci.* **1985**, *149*, 366. Meyer, R. J.; Duke, C. B.; Poton, A.; Kahn, A.; So, E.; Yeh, S. L.; Mark, P. *Phys. Rev. B.* **1979**, *19*, 5194.
(89) Camillone, N., III; Khan, K. A.; Yarmoff, J. A.; Osgood, R. M., Jr. *Phys. Rev. Lett.* **2001**, *87*, 056101.
(90) Rous, P. J. *Phys. Rev. Lett.* **1995**, *74*, 1835.
(91) Dobrin, S.; Lu, X.-K.; Naumkin, F. Y.; Polanyi, J. C.; Yang, J. *Surf. Sci.* **2004**, *573*, L363.
(92) Osgood, R. M., Jr.; Deutsch, T. F. *Science* **1985**, *227*, 709.
(93) Fairbrother, D. H.; Briggman, K. A.; Stair, P. C.; Weitz, E. *J. Phys. Chem.* **1994**, *98*, 13042.
(94) Garrett, S. J.; Holbert, V. P.; Stair, P. C.; Weitz, E. *J. Chem. Phys.* **1994**, *100*, 4615.

(95) Holbert, V. P.; Garrett, S. J.; Stair, P. C.; Weitz, E. *Surf. Sci*. **1996**, *346*, 189.
(96) Polanyi, J. C.; Sze, N. S.-K.; Wang, J.-X. *J. Phys. Chem. A* **1997**, *101*, 6679.
(97) Ashfold, M. R.; Howe, J. D. *Annu. Rev. Phys. Chem*. **1994**, *45*, 57. Friedrich, D. M.; McClain, W. M. *Annu. Rev. Phys. Chem*. **1980**, *31*, 559.
(98) Srivastava, A.; Osgood, R. M., Jr. *J. Chem. Phys*. **2003**, *119*, 10298. Srivastava, A.; Osgood, R. M., Jr. *Chem. Phys. Lett*. **2002**, *355*, 371.
(99) Kim, J.; Kelley, J. A.; Ayotte, P.; Nielson, S. B.; Weddle, G. H.; Johnson, M. A. *J. Am. Soc. Mass Spectrom* **1999**, *10*, 810.
(100) Maksymovych, P.; Sorescu, D. C.; Dougherty, D.; Yates, J. T., Jr. *J. Phys. Chem. B* **2005**, *109*, 22463.
(101) Camillone, N., III; Khan, K. A. *Surf. Sci*. **2000**, *453*, 85.
(102) Camillone, N., III; Adib, K.; Khan, K. A.; Mocuta, D.; Osgood, R. M., Jr. *J. Phys. Chem B* **2002**, *106*, 12491.
(103) Cui, X. D.; Primak, A.; Zarate, X.; Tomfohr, J.; Sankey, O. F.; Moore, A. L.; Moore, T. A.; Gust, D.; Harris, G.; Lindsay, S. M. *Science* **2001**, *294*, 571.
(104) Ulman, A. *An Introduction to Ultrathin Organic Films*: *From Langmuir Blodgett to Self-Assembly*; Academic Press: Boston, 1991. Lercel, M. J.; Craighead, H. G.; Parikh, A. N.; Seshadri, K.; Allara, D. L. *Appl. Phys. Lett*. **1996**, *68*, 1504; *J. Vac. Sci. Tech. B* **1994**, *12*, 3663.
(105) Olsen, C.; Rowntree, P. A. *J. Chem. Phys*. **1998**, *108*, 3750.
(106) Camillone, N., III; Khan, K. A.; Osgood, R. M., Jr. *Surf. Sci*. **2000**, *453*, 85.
(107) Vaghjani, G. L. *J. Chem. Phys*. **1993**, *99*, 5936.
(108) Chen, C. J.; Osgood, R. M., Jr. *Phys. Rev. Lett*. **1983**, *50*, 1705. Chen, C. J.; Gilgen, H. H.; Osgood, R. M., Jr. *Opt. Lett*. **1985**, *10*, 173.
(109) Schwartz, W. N.; Yang, Q. Y.; Chen, D. L.; Osgood, R. M., Jr. *J. Chem. Phys*. **1992**, *97*, 722.
(110) Phillips, H. R.; Ehrenreich, H. *Phys. Rev*. **1963**, *129*, 1550.
(111) Podlesnik, D. V.; Gilgen, H. H.; Willner, A. E.; Osgood, R. M., Jr. *J.O.S.A. B* **1986**, *3*, 775.
(112) Nordlander, P.; Tulley, J. C. *Phys. Rev. Lett*. **1988**, *61*, 990. Gadzuk, J. W. Annu., *Rev. Phys. Chem*. **1988**, *39*, 395. Gadzuk, J. W.; Richter, L. J.; Buntin, S. A.; King, D. S.; Cavanagh, R. R. *Surf. Sci*. **1990**, *235*, 317.
(113) Bourdon, E. B. D.; Das, P.; Harrison, I.; Polanyi, J. C.; Segner, J.; Stanners, C. D.; Williams, R. J.; Young, P. A. *Faraday Discuss. Chem. Soc*. **1986**, *82*, 343. Harrison, I.; Polanyi, J. C.; Young, P. A. *J. Chem. Phys*. **1988**, *89*, 1475.
(114) Fairbrother, D. H.; Briggman, K. A.; Stair, P. C.; Weitz, E. *J. Chem. Phys*. **1995**, *102*, 7267.
(115) Garrett, S. J.; Holbert, V. P.; Stair, P. C.; Weitz, E. *J. Chem. Phys*. **1994**, *100*, 4626.
(116) McCarthy, M. I.; Gerber, R. B.; Trentelman, K. A.; Strupp, P.; Fairbrother, D. H.; Stair, P. C.; Weitz, E. *J. Chem. Phys*. **1992**, *97*, 5168.
(117) McGlynn, S. P.; Smith, F. J.; Cilento, G. *Photochem. Photobiol*. **1964**, *3*, 269.
(118) Jensen, E. T.; Polanyi, J. C. *J. Chem. Phys*. **1993**, *97*, 2257.
(119) Huang, Z. H.; Guo, H. J. *Chem. Phys*. **1993**, *98*, 7413.
(120) Huang, Z. H.; Guo, H. J. *Chem. Phys*. **1993**, *98*, 3395.
(121) Kutzner, J.; Lindeke, G.; Welge, K. H.; Feldman, D. *J. Chem. Phys*, **1989**, *90*, 548.
(122) Guo, H.; Schatz, G. *Chem. Phys. Lett*. **1991**, *184*, 245.
(123) Kim, S. H.; Briggman, K. A.; Stair, P. C.; Weitz, E. *J. Vac. Sci. Technol*. **1996**, *A14*, 1557.
(124) Henderson, M. A.; White, J. M.; Uetsuka, H.; Onishi, H. *J. Am. Chem. Soc*. **2003**, *125*, 14974.
(125) Henderson, M. A.; Epling, W. S.; Peden, C. H. F.; Perkins, C. L. *J. Phys. Chem. B* **2003**, *107*, 53.
(126) Perkins, C. L.; Henderson, M. A. *J. Phys. Chem. B* **2001**, *105*, 3856.
(127) Onda, K.; Li, B.; Petek, H. *Phys. Rev. B* **2004**, *70*, 045415.
(128) Onda, K.; Li, B.; Zhao, J.; Jordan, K. D.; Yang, J.; Petek, H. *Science* **2005**, *308*, 1154.
(129) Onda, K.; Li, B.; Petek, H. In *Ultrafast Phenomena XIV*; Kobayashi, T. O., Nelson, K., DeSilvestri, K., Eds.; Springer-Verlag: Berlin, 2005.
(130) Li, B.; Zhao, J.; Onda, K.; Jordan, K.; Yang, J.; Petek, H. *Science* **2006**, *311*, 1436.
(131) Wendt, S.; Schaub, R.; Matthiesen, J.; Vestergaard, E. K.; Wahlstrom, E.; Rasmussen, M. D.; Thostrup, P.; Molina, L. M.; Laegsgaard, E.; Stensgaard, I.; Hammer, B.; Besenbacher, F. *Surf. Sci*. **2005**, *598*, 226.
(132) Totir, G. G.; Le, G. Y.; Osgood, R. M., Jr. *J. Phys. Chem. B* **2005**, *109*, 8452.
(133) Lu, P. H.; Lasky, P. J.; Yang, Q.-Y.; Osgood, R. M., Jr. *Chem. Phys*. **1996**, *205*, 143.
(134) Zhou, X. L.; Solymosi, F.; Blass, P. M.; Cannon, K. C.; White, J. M. *Surf. Sci*. **1989**, *219*, 294.
(135) Black, J. F.; Powis, I. *Chem. Phys*. **1988**, *125*, 375.
(136) Huang, W. X.; White, J. M. *J. Phys. Chem. B* **2004**, *108*, 5060.
(137) Jo, S. K.; White, J. M. *J. Phys. Chem*. **1990**, *94*, 6852.
(138) Zhou, X. L.; Zhu, X. Y.; White, J. M. *Surf. Sci. Rep*. **1991**, *13*, 73.
(139) Brown, G. E.; Henrich, V. E.; Casey, W. H.; Clark, D. L.; Eggleston, C.; Felmy, A.; Goodman, D. W.; Gratzel, M.; Maciel, G.; McCarthy, M. I.; Nealson, K. H.; Sverjensky, D. A.; Toney, M. F.; Zachara, J. M. *Chem. Rev*. **1999**, *99*, 77.
(140) Dobrin, S.; Harikumar, K. R.; Matta, C. F.; Polanyi, J. C. *Surf. Sci*. **2005**, *580*, 39.
(141) White, J. D.; Chen, J.; Matsiev, D.; Auerbach, D. J.; Wodtke, A. M. *Nature* **2005**, *433*, 503.

CR050175X